3-11-2011

Radial Distribution of Absorption in a Cesium Heat Pipe with Axial Laser Heating

Charles D. Fox

RADIAL DISTRIBUTION OF ABSORPTION IN A CESIUM HEAT PIPE WITH AXIAL LASER HEATING

THESIS

Charles D. Fox

AFIT/GAE/ENY/11-M09

DEPARTMENT OF THE AIR FORCE
AIR UNIVERSITY
AIR FORCE INSTITUTE OF TECHNOLOGY
Wright-Patterson Air Force Base, Ohio

AFIT/GAE/ENY/11-M09

RADIAL DISTRIBUTION OF ABSORPTION IN A CESIUM HEAT PIPE WITH AXIAL LASER HEATING

THESIS

Presented to the Faculty

Department of Aeronautics and Astronautics

Graduate School of Engineering and Management

Air Force Institute of Technology

Air University

Air Education and Training Command

In Partial Fulfillment of the Requirements for the

Degree of Master of Science in Aeronautical Engineering

Charles D. Fox

March 2011

AFIT/GAE/ENY/11-M09

RADIAL DISTRIBUTION OF ABSORPTION IN A CESIUM HEAT PIPE WITH AXIAL LASER HEATING

Charles D. Fox

Approved:

_____	_____
Glen P. Perram, (Chairman)	Date
_____	_____
Dr. Marc D. Polanka, (Member)	Date
_____	_____
Dr. Mark F. Reeder (Member)	Date

Abstract

Diode Pumped Alkali Lasers (DPAL) have been scaled to greater than 100 W and exhibit slope efficiencies exceeding 80%, offering application for tactical laser weapons. The hybrid DPAL system combines efficient diode pumping with the good beam quality and thermal characteristics of gas lasers. Thermal effects on alkali concentration have been observed to degrade performance, while low speed flowing systems are in development. However, spatial gradients in temperature and concentrations have not previously been observed. In the present work, a 0.8 W/cm^2 pump laser at the D_1 frequency heats the medium in a T=50-100˚C cesium heat pipe with 5 Torr nitrogen used for quenching. A 31 μW/cm^2 diode laser probes the spectral absorbance of the cesium cell on the D_2 transition with radial spatial resolution. The 300 kHz linewidth probe laser is scanned 20 GHz across the optically thick hyperfine structure, revealing absorbances of 1-5. The absorbance outside of the pumped volume is modulated by up to a factor of 2 when the pump beam is blocked, suggesting significant temperature gradients. The radial temperature profile is observed across the 1.5 cm pipe with resolution of 2 mm. The variation of pump power, nitrogen pressure, and heat pipe temperature has been provided showing distinct trends. Cesium D_2 lineshapes have been obtained for several heat pipe spatial locations with the pump laser actively heating the gaseous medium.

Acknowledgments

I would like to thank Dr. Glen Perram, my thesis advisor, for his time and effort devoted to this research. His guidance through experimental problem solving is greatly appreciated. Mike and Greg are also thanked for their assistance with lab equipment and guidance through procedures. Dr. Pitz, Dr. Sulham, and Chris Rice have taught me a number of things leading to this research being possible. I would remise not to thank my family for their support. The Air Force Office of Scientific Research and The High Energy Laser Joint Technology Office are also thankfully acknowledged for making these demonstrations possible.

Charles D. Fox

Table of Contents

List of Figures

Page

List of Equations

List of Abbreviations

ABL	Airborne Laser
ATL	Advanced Tactical Laser
COIL	Chemical Oxygen Iodine Laser
DoD	Department of Defense
DoE	Department of Energy
DPAL	Diode Pumped Alkali Laser
DPSSL	Diode Pumped Solid State Laser
FWHM	Full Width at Half Max
HEL	High Energy Laser
USAF	United States Air Force

Nomenclature

Symbol	Description
A	Absorbance
$\bar{A}$	Average Absorption
α	Absorption Coefficient
β	Constant
c	Speed
D_1	$^2P_{1/2} \rightarrow {}^2S1_{/2}$
D_2	$^2S_{1/2} \rightarrow {}^2P_{3/2}$
dT/dx	Thermal Gradient
f_o	Constant
I_o	Reference Intensity
I_t	Transmitted Intensity
K, k	Thermal Conductivity
k_o	Reference Thermal Conductivity
L	Cell Length
L_a	Adiabatic Length
L_c	Condenser Length
L_e	Evaporator Length
n	Number Density
P	Pressure
P’	Pressure and Change in Pressure
P_{in}	Incident Power
ΔP	Change in Pressure
q	Heat Flux
q_v	Heat Power Deposited
r	Radius
σ	Cross Section
T	Temperature
T_o	Reference Temperature
u	Direction unit vector
ν	Frequency
$\Delta\nu_D$	Doppler FWHM
$\Delta\nu_L$	Lorentzian FWHM
W	Watts
w_p	Beam Waist Radius

RADIAL DISTRIBUTION OF ABSORPTION IN A CESIUM HEAT PIPE WITH AXIAL LASER HEATING

I. Introduction

1. Background

Diode Pumped Alkali Lasers (DPALs) have recently been demonstrated in many research efforts. Krupke in 2003 first produced a rubidium alkali laser pumping on the D_2 line ($^2S_{1/2} \rightarrow {}^2P_{3/2}$) and lasing on the D_1 line ($^2P_{1/2} \rightarrow {}^2S1_{/2}$) [1]. The small energy defect between the excited states in the alkalis leads to the use of these types of elements commonly in the DPAL community. The DPAL is a three level optically pumped laser system, with one of the alkalis as the gaseous medium, and was given its name by Beach [2].

The Department of Defense has been interested in High Energy Lasers (HEL) leading to the research and development carried out over the past several years. There are two well known lasers that have developed known as the Chemical Oxygen Iodine Laser (COIL) and Diode Pumped Solid State Lasers (DPSSLs). The COIL is a highly efficient system that has achieved tasks strategically and tactically on board the advanced tactical laser (ATL) and the Airborne Laser (ABL) [14]. A USAF C-130 fitted with the COIL laser system has shown abilities to destroy missiles on more than one occasion which only enhances the deployability of this type laser system. This laser has accomplished powers on the order of a megawatt while the system does have two main disadvantages. The COIL requires non common battlefield chemicals that leave long logistical trails and the usage time is limited to the onboard chemical supply.

The second well known laser system, known as DPSSL, is driven by the disadvantages of the COIL and the increase of Air Force interest in lasers as a defensive weapon system. The DPSSLs are capable of having an unconstrained amount of laser shots due the elimination of the chemicals and incorporation of electrically pumped diodes [14]. However DPSSLs have thermal management issues due to the solid state gain medium which limits this laser system to current heat transfer technology. This laser has been shown to be effective at powers around 100kW in the most recent demonstrations [11].

Current research increases have began the development of a laser that includes the advantages of the COIL and DPSSL as well as attempt to eliminate the thermal effects and limited laser shots. The DPAL system has evolved from these design constraints and has began to give promising results for future implementation to modern warfare. The DPAL has been demonstrated at laser powers higher than 100W [16]. Although the DPAL has only been around for a short time, the technologies and research techniques of the COIL and DPSSLs have guided the development process. The Department of Defense (DoD), Department of Energy (DoE), and Air Force combined efforts have given DPALs the possibility of becoming a feasible, deployable, and efficient HEL.

2. Motivation

Lasers have grown to be a desired asset for military operation and have performed in promising manners to provide a new battle field weapon. Modern warfare is beginning to change as all four branches of the United States Armed Forces are pursuing research and development of HEL weapons. The advancements have led to many valuable capabilities including: Destroying time critical targets, strategic capabilities, and inexpensive missions, and most importantly, a great increase in national security.

> "It isn't very often an innovation comes along that revolutionizes our operational concepts, tactics and strategies. You can probably name them on one hand - the atomic bomb, the satellite, the jet engine, stealth, and the microchip. It's possible the airborne laser is in this league."
>
> Sheila Widnall
>
> Former Secretary of the Air Force

3. Problem Statement

Gaseous mediums are sensitive to temperature gradients that could create large number density differences in an enclosed volume. The total gaseous volume is considered to be in equilibrium and hold a constant number density throughout the volume until a laser load interrogates the medium. At this point, part of the total molecules, the molecules inside the loaded volume, are heated and therefore a number density gradient in the entire volume. The density gradients are considered unfavorable and current day to day calculations assume constant number densities when laser loads are present.

The unknowns prior to this research include the magnitude of the thermal gradients when a laser load is present and heating a portion of the gaseous medium. If the laser load were to decrease the number density in the loaded volume and force an increase in number density elsewhere, then this is a potential problem. The sole purpose of the alkali gaseous mediums utilized in DPAL systems is to interact with the alkali while an

interaction naturally will heat the interrogated volume and could significantly affect the number density within the loaded volume.

The significance of thermal management has been mentioned about the Diode Pumped Alkali Lasers by several including Zhu [3]. The vast majority of the thermal management problems are predicted to occur when scaling the DPAL system to the multi-kilowatt or megawatt power class. Heat transfer theories about natural equilibrium provide strong evidence that the axial laser load could be the main driver for significant differences in alkali concentration throughout a heat pipe with a gaseous medium. The internal thermal resistance models with geometry of concentric pipes serve as a rough baseline for the experimental results provided by Mills [4].

A gaseous medium increases the complexity of the thermal conductivity while solid and liquid mediums have negligible differences throughout the volume. Viscous flow theories aid in the modeling by providing equations for thermal conductivity as a function of temperature, White [5]. A second order non-linear differential equation can be used to model the radial temperature profile that develops due to the axial laser load [3].

4. Research Objectives

The main objective of this research is to experimentally determine if an axial laser load significantly influences the thermal gradients in the gaseous medium while a portion of the medium is interrogated via a laser load. The data will be matched qualitatively and quantitatively to past research to baseline the experiment. The comparison of a current model incorporating the main dependent variables driving the thermal gradients allows for several future projections for the DPAL community. Aiding the DPAL research by

providing additional experimental results will strengthen predictions as to what to prepare prior to scaling and implementation.

5. Overview of Thesis

This document begins with a review of thermal management in lasers that have developed and could be a potential problem when scaling the DPAL system. Chapter II also includes information on gaseous medium behaviors, thermal influence on lineshapes, and equations to explain the lineshapes. Chapter III clearly spells out the experimental setup specifics to ensure proper and repeatable measurements of the thermal gradients due to the axial laser load. The results provided in chapter IV give evidence that thermal gradients are significant while various temperatures, lineshapes as a function of heat pipe location, pump powers, and nitrogen pressures are shown to verify trends. The current modeling efforts in Chapter V are compared to the experimental data while alternative calculations are attempted to provide quantitative values for the temperature throughout the gaseous medium. The conclusions found give additional support to laser driven number density gradients do indeed exist and the significance of the laser induced number density distributions.

II. Background

1. DPALs

The DPAL has been shown to operate efficiently at powers higher than 100W [16] while maintaining slope efficiencies over 80% [14] bringing promising scaling performance. The DPAL competes with the COIL and DPSSL due to the performance characteristics shown in the recent demonstrations. Although DPALs are still young, the research and development has been fueled by the capabilities previously shown by the COIL. DPALs are currently researched across the world and have a strong interest by the United States Air Force for the deployment of a strategic and tactical HEL weapon.

The DPAL systems are comprised of characteristics from both the COIL and the DPSSLs. The high heat created by the DPSSLs and time between laser shots limits its

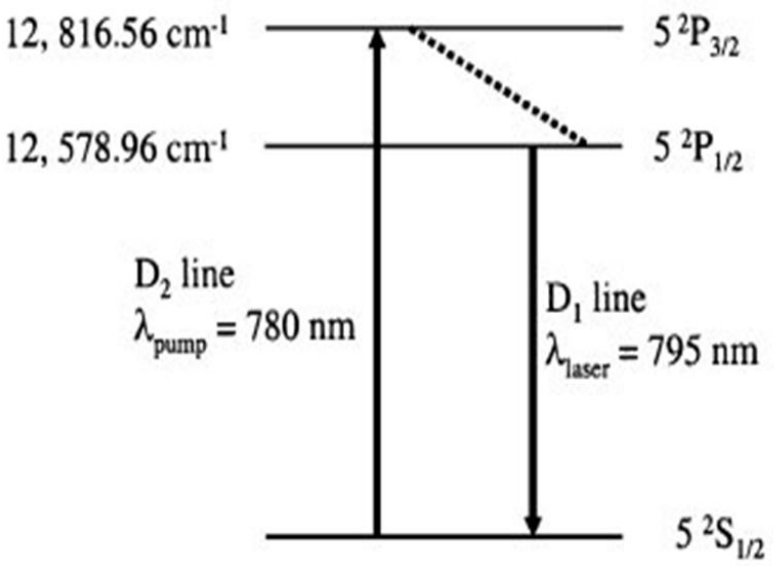

Figure 1: Krupke's Rb DPAL Energy Diagram[1]

scaling while the COIL requires uncommon battlefield chemicals and has a limited magazine depth. The DPAL is a gas phase laser that has been shown to perform well at mid-range powers and will be scaled to higher range powers in the near future. Good

beam quality, promising slope efficiencies, and the simplicity of the DPAL system give insight for a compact and deployable laser weapon.

Krupke's first DPAL system, shown in Figure 1, pumps alkali atoms from the $^2S_{1/2}$ ground state up to the $^2P_{3/2}$ second excited state known as the D_2 line. The atoms are then collisionally relaxed from the $^2P_{3/2}$ second excited state to the $^2P_{1/2}$ excited state. The atoms then return to the $^2S_{1/2}$ ground state from the $^2P_{1/2}$ excited state known as the D_1 line [1]. Similar transitions are possible with all the alkalis as given in Table 1 [11]. The cesium energy defect for cesium is much larger than that of the other alkalis.

Table 1. Alkali D_1 and D_2 transition wavelengths and fine structure splitting [11]

Alkali	D_1 (laser) (nm)	D_2 (pump) (nm)	ΔE ($^2P_{3/2} - {}^2P_{1/2}$) (cm^{-1})
Li	670.98	670.96	0.444
Na	589.76	589.16	17.2
K	770.11	766.70	57.7
Rb	794.98	780.23	237
Cs	894.59	852.35	554

The DPAL demonstrations in this work utilized cesium alkali similar to the transitions of rubidium in that it is also a three level laser operating between the same excited states. The $^2S_{1/2}$ ground state atoms are pumped up to the $^2P_{3/2}$ second excited state, then spin orbit relaxed to the $^2P_{1/2}$ excited state. The atoms then lase along the D1 line back to the ground state.

2. Thermal Management in DPALs

Past HELs have been faced with thermal management problems that can be detrimental to the performance characteristics when scaling. The low power systems operate in a regime where thermal effects are small and considered insignificant to research. The high powers required to destroy targets brings high thermal loads on the gaseous mediums and components of the laser systems. The solid state lasers have shown to have major problems in scaling due to the inability to dissipate the waste heat while gaseous mediums have shown to remove the heat much more effectively.

In DPAL systems, the studied thermal aspect evolves from the use of a medium that allows for thermal gradients to develop. A laser interrogated gaseous medium will naturally have a new thermal profile. Prior to the laser being present in the medium, the medium can be considered to have rather uniform properties. The medium must be interrogated with a laser properly tuned to that of the absorption wavelength of the gas used. For the research presented, the gaseous medium is cesium while the laser is tuned to the D_1 line for cesium mentioned later.

Pulsed and CW DPALs have been compared in recent demonstrations by Zhdanov et al [17]. The input versus output power is given showing that there appears to be some limit to the CW DPAL. The pulse duration of 100 ms and repetition rate of 1 Hz was used to generate a pulsed system DPAL [17]. The slope of the input versus output power for the pulsed system appears to be linear while the CW has a visible maximum. This suggests a cooling time is required to allow the DPAL system to dissipate heat as the pulsed system behaves. The Appendix contained these demonstrations in Figure 34.

The molecules inside the interrogated region will move to a higher energy excited state. The molecule will then either relax by additional collisions with an additional added gas or naturally radiate back to the ground state. Nitrogen is added to the heat pipe in the studies carried out in this work. The nitrogen will receive the energy from the cesium atom, therefore increasing the temperature of the interrogated volume. While this interrogated volume becomes heated, the velocity of the atoms in this region will increase and therefore decrease the local number density. The heated atoms will move outside the interrogated region and increase the number density outside of the heated region.

A process termed "Thermophoresis" relates well with the thermal gradients present in this work. The thermal forces acting on gas particles that have temperature gradients are presented by Bird [6]. The forces originate from the Chapman-Enskog distribution:[6]

$$f = fo\left\{1-\frac{4}{5}\frac{\beta^2 K}{RT}\left(\beta^2 c^2-\frac{5}{2}\right)u\frac{dT}{dx}\right\} \qquad (1)$$

where dT/dx is the thermal gradient, T is the temperature, R is the gas constant, K is the Boltzman's constant, f_o is a constant, β is a constant, and c is the speed. The thermal gradient driving the molecular forces can be observed from this equation noting that there is a direct relationship between the gradient and force. This equation applies to this work by which the heat pipe number density distribution is related to the thermal gradient.

A technique used in many heat transfer solid models is two concentric pipes of two different temperatures, as shown in Figure 2. The inner pipe can be given a temperature different from the outer pipe. The medium between the two is often solid and the inner pipe is usually given a boundary temperature. Thermal resistance methods are often used to determine the linear temperature distribution throughout the material or at its external

surface. The thermal solutions for this, although semi-accurate for solids and liquids, are far from the behavior of a gaseous medium. The linear equation often used in basic heat transfer analysis is given by Equation 2:[4]

$$q = -k\frac{dT}{dx} \tag{2}$$

where k is the thermal conductivity and dT/dx is the thermal gradient. This equation provides information about the gradient as well as close temperature approximations for points throughout [4]. The heat flux denoted by q is equal to the thermal conductivity multiplied by the thermal gradient. The distance between the two temperatures must be known as well as one of the temperatures at the boundary of the thermal gradient to

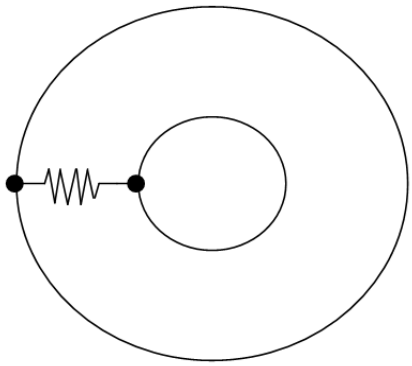

Figure 2: Concentric Pipes

determine the other boundary. In section 5 of this chapter, a current second order nonlinear differential equation is used to model the complex gaseous medium behavior.

3. Absorption Regime

The well known Beer's Law equation is often applicable for basic absorption calculations for DPAL systems. Photons entering a gaseous medium are absorbed moving population to a higher state of energy. The absorbance equation is given as:[7]

$$A = \sigma \, \mathrm{n} \, \mathrm{l} = -\ln \frac{I_t}{I_o} \tag{3}$$

Where σ is the cross section, n is the number density, l is the length, I_t is the transmitted intensity, and I_o is the incident intensity. The heat pipe alkali length is approximately 10 cm determined from the length of the heated region described in chapter 3. The cesium cross section denoted by σ is taken to be 1.5×10^{-15} m^2 at 10 Torr provided by Pitz [8]. A known heat pipe external temperature of 70˚C leads to the estimation of the heat pipe number density. Steck gives the approximated number density at 343 K to be 1.7×10^{14}. These three variables can be used to determine an absorbance denoted by A. The experimental work provided has shown values of absorbance ranging from 0-8 while greater values are lost due to the low signal to noise.

4. Heat Pipe Concept

The heat pipe has been used in many applications and is not considered a new technology by any means. The heat pipe concept has been traced back as far as the 1800's to patents of A.M. Perkins and J. Perkins [9]. The designs of this time consisted of an evaporator and condenser region with transport between the two regions by using the phase change as mentioned by Peterson [9]. The recent increased used of heat pipes in DPALs has introduced the capacity to demonstrate high temperature and high pressure experiments. Heat pipes are often used in space applications and have provided a method to transfer energy from one location to another through natural phenomenon. They have also been used for thermal control of nuclear reactors, electronic devices, and bring advantages in the Alaskan pipeline.

The internal complexity of the heat pipe can be designed in several different ways and can have many different kinds of mediums. The work presented uses cesium as the gaseous medium with 5 Torr N_2. The capillary pumping from the condenser to the evaporator region is made possible through wicks, grooves, or small pipe diameters. The pipe itself can be constructed of many materials. For high temperatures metals are desired due to the high boiling point and structural rigidity when operating at very high

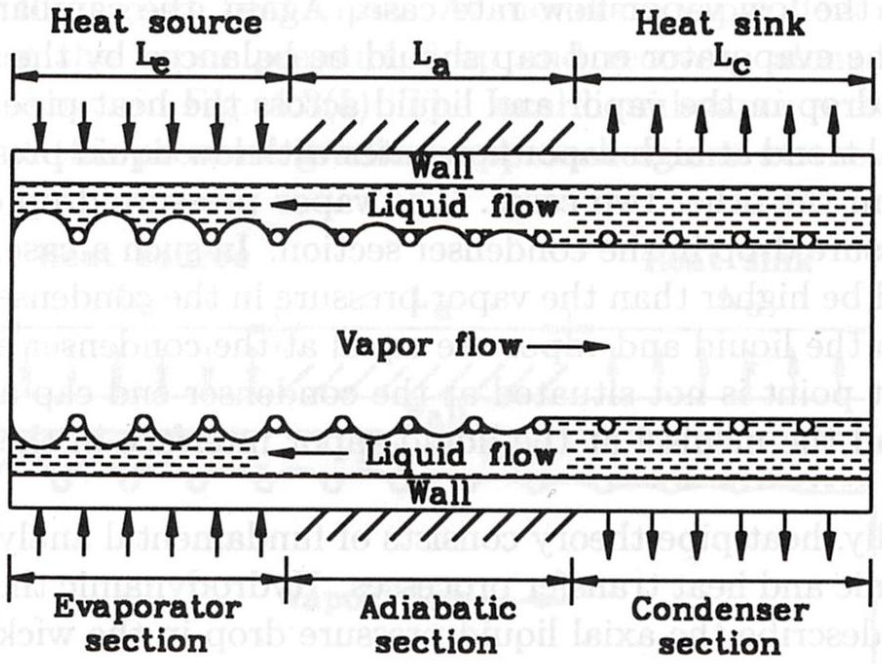

Figure 3: Heat Pipe Schematic[12]

pressures and temperatures. The thermal regions can be better understood by observations from Figure 3, which shows the internal complexities. Faghri has tabulated wick designs and suggestive materials for heat pipe fabrication and gives insight as to the length of the condenser region for operation temperature differences [10]. The construction of the heat pipe is quite tedious and small errors in assembly could require rebuilding.

5. Modeling Thermal Profiles in DPALs

The complex gaseous medium thermal gradients have not yet been experimentally shown and have only been predicted by several. A second order nonlinear differential equation has been provided by Zhu to attempt to predict the behavior of the alkali volume interrogated [3]. The model assumes a Gaussian beam that incorporates not only the radial thermal gradients, but also the longitudinal thermal gradients. The modeled pump laser is located on axis of the interrogated gaseous medium. The alkali is modeled as cesium with 500 Torr helium gas. The radial and longitudinal thermal gradients are described by the steady state heat conductive equation:[3]

$$\nabla \bullet (k \nabla T(r,z)) + q_v = 0 \tag{4}$$

A separation of variables technique is used introducing two main constants to be varied depending on the experiment. The thermal conductivity is given as:[3]

$$k = 0.0015\sqrt{\frac{T}{273}} \tag{5}$$

is shown in equation 5, is proportional to the square root of temperature and has a constant according to the 500 Torr of Helium used in Zhu's model. The heat deposited exponentially changes as propagating down axis while also exponentially decreasing from the centerline axis to the cell walls. The heat deposited is given by:[6]

$$q_v = \frac{2\alpha\eta_h P_{in} e^{\frac{-2r^2}{w_p{}^2}} e^{-\alpha(z+0.01)}}{\pi w_p{}^2} \tag{6}$$

where α is the absorption coefficient, η_h is an efficiency factor, P_{in} is the power in, w_p is the beam waist radius, z is the cell length, and r is the cell radius.

The boundary conditions given in equation 7 are utilized by Zhu to generate the solution shown in figure 4. The temperature at the edges of the pump beam is also assumed to be equal but remain unknown prior to generating a solution. Figure 4 is a graphical representation of the model predictions for the specifics mentioned and discussed in more detail by Zhu [3]. The pump power was assumed to be 40 W, an absorption coefficient of 70 %, cell length of 2 cm, and cell radius of 2 cm.

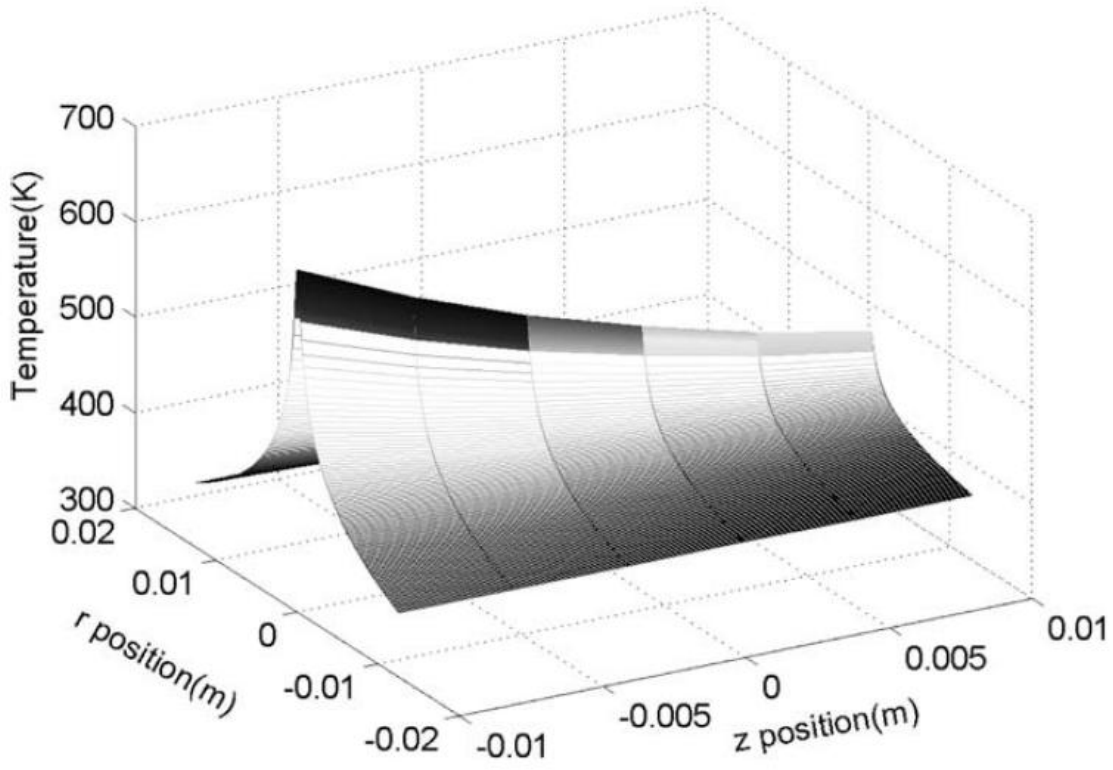

Figure 4: Model Thermal Gradient Predictions

The second order nonlinear differential equation used in the past work to model the DPAL system is given as:[3]

$$\frac{d^2T}{dr^2}+\frac{1}{r}\frac{dT}{dr}+\frac{1}{2T}\left(\frac{dT}{dr}\right)^2+\frac{q_v}{k}=0$$
$$\frac{dT}{dr}=0 \quad @ \quad r=0\,mm \tag{7}$$
$$T=70C \quad @ \quad r=7.5\,mm$$

where r is the radius and T is the temperature. The solution to Equation 7 provides a prediction to the magnitude of the thermal gradients that are present in DPAL systems. Although not yet demonstrated experimentally, the model gives good indication for the existence of strong thermal gradients. Zhu provides several plots varying the pump power, radial distance, absorption coefficients, beam waists, all leading to predicted high thermal gradients within the gaseous medium. The predicted gradients range from 800 K inside the pump beam while only 300 K at the cell walls. This large thermal gradient allows for alkali to leave the pump beam volume and therefore degrade performance.

6. Gaussian/Doppler, Lorentzian, and Voigt lineshapes

The Gaussian/Doppler and Lorentzian lineshapes are convolved to form the Voigt lineshape. The Gaussian is temperature dependant while the Lorentzian is pressure dependant. The Voigt lineshape is a representation of the range of frequencies that are capable of transitioning an atom from one energy level to another. In the DPAL system the addition of pressure and increase in temperature allow for a lineshape to match the pump linewidth. The pump leakage between the Voigt lineshape and the pump lineshape is a deficiency in the laser as described by Sulham [11]. If the pressure is held constant

and only the temperature is able to fluctuate, then the Lorentzian part of the Voigt will remain unchanged while the Gaussian part will undergo thermal dependant changes [7].

The Gaussian lineshape formulation is given as:[7]

$$g_D(\nu) = \frac{2}{\Delta\nu_D}\sqrt{\frac{\ln 2}{\pi}}e^{\frac{-2(\nu-\nu_O)}{\Delta\nu_D}\ln 2} \tag{8}$$

where $\Delta\nu_D$ is the FWHM, ν is the frequency, and ν_o is reference frequency. The FWHM can be calculated from:

$$\Delta\nu_D = 2\nu_o\sqrt{\frac{2kT\ln 2}{mc^2}} \tag{9}[7]$$

where k is the Boltzman's constant, T is temperature, m is the mass, and c is the speed of sound. This value for a temperature of 343 K, mass of 132.9 amu (cesium), and reference frequency of 351725.7 yields a FWHM of approximately 380 MHz. The thermal gradients that can be developed in DPALs can result in different Gaussian lineshapes throughout the gaseous volume. The frequency required to excite the cesium could be broadened and/or shifted according the strength of the thermal gradients. The scaled or shifted lineshape could be a potential degradation in performance of the DPAL system.

The Lorentzian part of the Voigt lineshape is dominated by the pressure of the gaseous medium [7]. The thermal changes will directly relate to the number density while pressure is considered to remain constant throughout the medium. The Lorentzian lineshape is given as:[7]

$$g_L(\nu) = \frac{\frac{2}{\pi \Delta \nu_L}}{1 + \left[\frac{2(\nu - \nu_o)}{\Delta \nu_L}\right]^2} \tag{10}$$

where ν is the frequency and $\Delta\nu_L$ is the Lorentzian FWHM. The FWHM can be expressed as:[7]

$$\Delta \nu_L = \frac{1}{2\pi}\left(\frac{1}{\tau_r} + k_p p\right) \tag{11}$$

where τ_r is the radiative lifetime, and P is the pressure. For a pressure of 5 Torr N_2 and a radiative lifetime of 34.8, the Lorentzian width is approximately 12 MHz. An important note about the temperature variation with constant pressure is necessary to mention. The convolution of the two is the true lineshape, while if only temperature is changing, the Gaussian part will change. The normalized comparison between the Gaussian and Lorentzian lineshapes is shown in Figure 5 provided by Bernath [7]. The amplitude of the Gaussian is much higher than the Lorentzian. The important and very significant

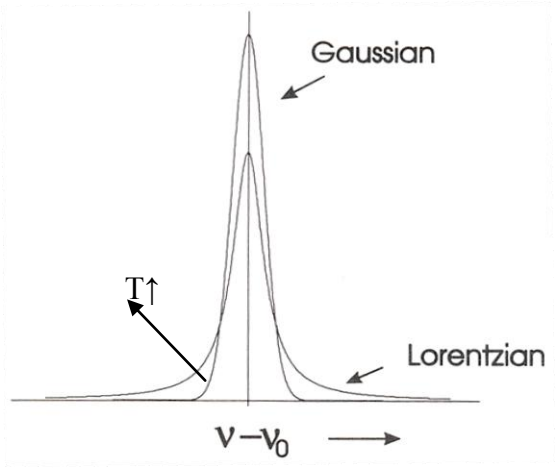

Figure 5: Lineshapes with Gaussian Thermal Dependence

detail to be noticed here is the wing on each side of the two lineshapes. If the pressure is held constant then the Lorentzian wing shape will remain the same while the Gaussian wings will rise and pass through the Lorentzian as temperature rises. Applied to DPALs, the thermal gradients that may exist will create a set of varying lineshapes throughout the gaseous medium.

III. Experimental

1. Energy Levels of Operation

The Cesium DPAL operates on the D_1 and D_2 lines and can be further understood through the energy diagram shown in Figure 6. The larger ground state spitting of $6^2S_{1/2}$ is 9192.6 MHz while the smaller $^2P_{1/2}$ is 1167.5 MHz as given by Andalkar [12]. The axial laser load, or pump beam, is populating the $6^2P_{1/2}$ while the probe populates the $6^2P_{3/2}$.

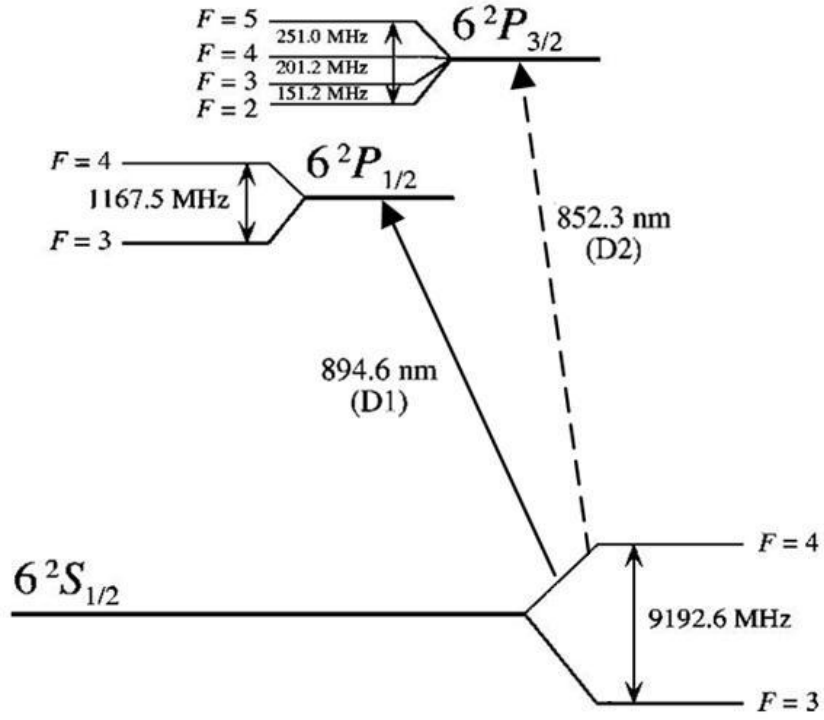

Figure 6: Energy Diagram for Pump and Probe

The Cesium alkali atoms are interrogated by a laser moving population from the $6^2S_{1/2}$ ground state to the $6^2P_{1/2}$ excited state. A separate laser moves population from the $6^2S_{1/2}$ ground state to the $6^2P_{3/2}$ second excited state. The population of the $6^2P_{1/2}$ excited state is achieved by a laser termed, the pump, along the D_1 line (894.6 nm) while the population of the $6^2P_{3/2}$ second excited state is achieved by a laser termed, the probe, along the D_2 line (894.3 nm). The pump and probe laser specifics are given in the following section.

2. Apparatus

The experimental apparatus is comparable to that of a typical DPAL system with a few unique characteristics to enable accurate and repeatable results. The pump beam is generated utilizing a Coherent MBR-110 Ti: Sapphire ring laser tuned near 894 nm. The MBR is pumped via a Coherent Verdi V-18 diode laser with a linewidth less than 100 kHz and wavelength near 532 nm. A New Focus Velocity tunable diode laser near 852 nm (model 6316) with a linewidth of less than 300 kHz provides the probing source with a maximum power of 100 mW. The pump beam powers are several orders of magnitude higher than the probe to avoid the probe influence on the gas medium to remain insignificant to the true thermal gradients. The probe beam power was greatly attenuated, less than 5 μW, prior to entry of the heat pipe to ensure Beer's law is applicable and to avoid saturation broadening. The pump spot size is approximately 2 mm in diameter, while the probe is also near to 2 mm is diameter. The pump and probe wavelengths/frequencies are monitored cautiously through two Bristol Wavemeters (model 621) to ensure proper spectral locations. Two Hamamatsu silicon photodiodes (model S2281-04) convert the probe reference (I_o) and transmitted (I) intensity in to

utilizable voltages as shown in Figure 7. These two modulated voltages are coupled to lock-in amplifiers with a reference frequency generated by a chopper rotating at 258 rpms. Two neutral density filters are employed to vary the pump and probe powers as necessary. The pump beam is assumed to be a Gaussian beam and has been focused through a convex lens to position the beam waist at the center of the heat pipe. The two motorized translation stages developed by Thorlabs (model MTS50-Z8E) allow for small displacements and repeatable spatial scans that are accurate to 10 μm, denoted by T.S., while the P.D. denotes the photodiodes.

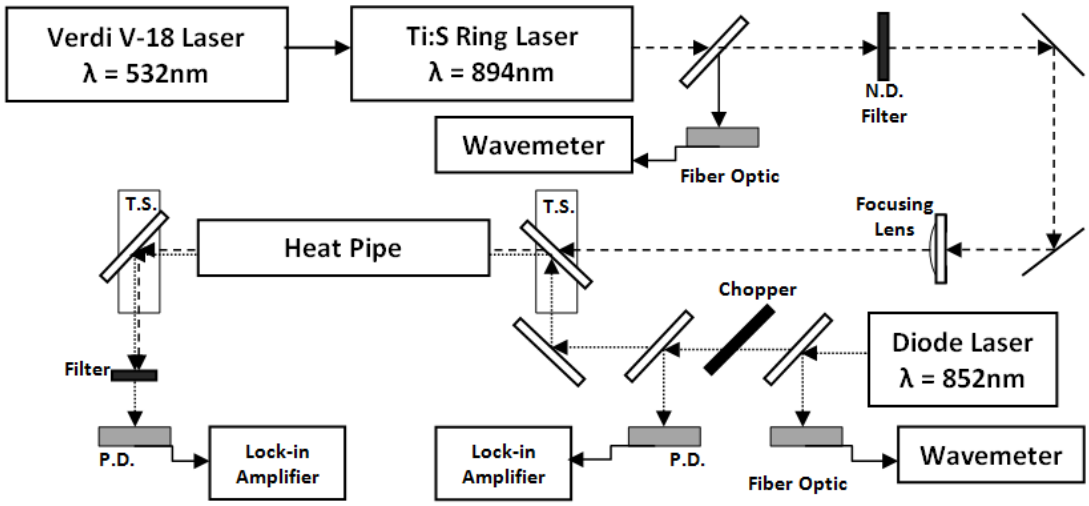

Figure 7: Experimental Apparatus Schematic

3. Heat Pipe Design and Operation

The heat pipe has many additional details that are essential to this experiment and critical to achieve normal DPAL operation. The pressure of the heat pipe was actively controlled by capacitance manometers (MKS model 690A) with 1, 10, and 100 Torr heads. A Watlow temperature controller (series SD) and 8 heater cartridges are utilized to actively regulate the heat pipe temperature while RTD's aid in recording the

temperature. The heat pipe constructed has three independently controlled temperature regions as shown in Figure 8. The ends of the heat pipe are held at 15˚C through two water cooling chillers manufactured by Neslab (model RTE-111), while the center is heated with the Watlow temperature controller. The ends of the heat pipe must be cooled to less than 29˚C, the boiling point of Cesium, to avoid deposits of Cesium from forming on the windows as mentioned by Sulham [11]. The ends of the heat pipe are often referred to as a condenser and the center an evaporator because of the gas medium phase changes occurring in these two distinct regions [4]. The internal complexity of the heat pipe contains a stainless steel wire mesh and spring, two copper crush gaskets, and Cesium alkali. The wire mesh is 150x150 strands per inch of stainless steel wrapped 4 times on the inner wall of the heat pipe, often called the wick. The wick is responsible for the capillary pumping of the Cesium from the condenser to the evaporator [4]. The spring is used to maintain a clear circular path through the heat pipe and secure the mesh. Two copper crush gaskets attach the Brewster angled windows to create a leak of less than 10^{-9} cc/sec. The heat pipe is then cleaned with Methanol followed by a baking

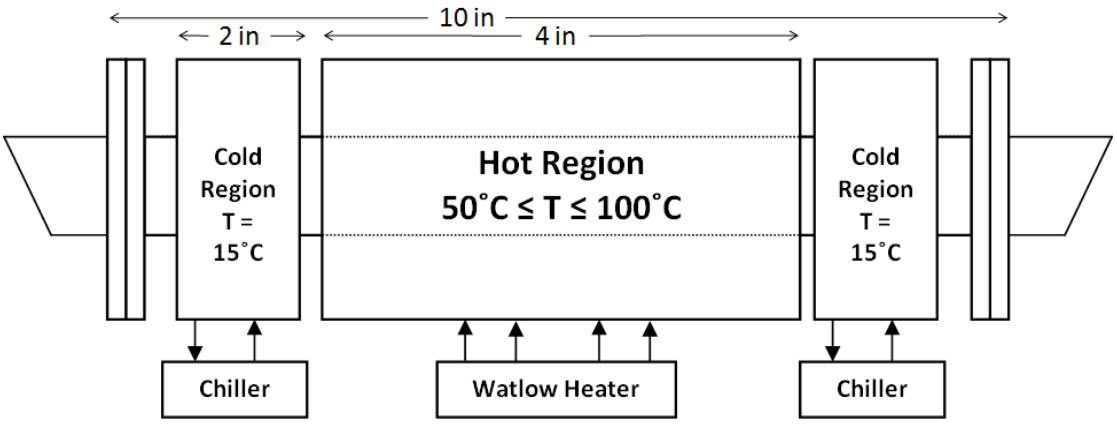

Figure 8: Heat Pipe Schematic of Operating Temperature Zones with Dimensions

process while under vacuum to remove any contaminants from the internal heat pipe volume. Two grams of 99.9 % pure solid Cesium Alkali is loaded into the center of the heat pipe while working inside a N_2 filled glove box. The heat pipe is then attached to the system shown in Figure 8 while the heat pipe volume is approximately 54.8 cm^2 while the system volume is approximately 154.19 cm^2. The N_2 added to the heat pipe has purity greater than 99.9 % and must be removed only when the heat pipe is cold.

The heat pipe cross-section shown in Figure 9 provides a visual of the pump location as well as divides the gaseous volume into two distinct regions. The spatial scans carried out start out with the probe laser at the left of region 1 and move through the gaseous medium and into region 2 where the pump beam is located. The Gaussian pump beam is positioned in region 2 to allow for probing of not only the heated volume to resolve the

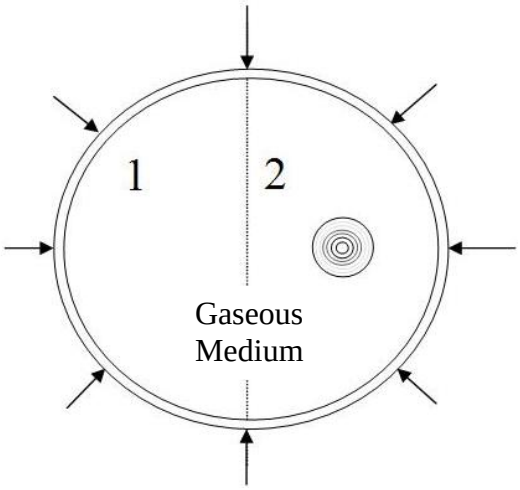

Figure 9: Internal Geometrical Setup

thermal gradients inside the pumped volume but also to resolve the thermal gradients throughout the entire gaseous medium. If the number density were to decrease inside region 2, then an increase in number density in region 1 must exist. The results show

how this fluctuation occurs instantaneously while the pump is turned off and on repeatedly across the cell in Chapter 4.

4. Spectral Locations

The heat pipe has been prepared with 5 Torr Nitrogen and heated to 70˚C in the evaporator region while the condenser is set to 15˚C. The pump and probe hyperfine structures have been pressure broadened very little and shifted even less. The x-axis in Figure 10 and Figure 11 is frequency that was obtained by converting the time axis to a frequency through the scan width and scan time which match the 5 Torr Nitrogen lineshapes given by Pitz [8,13]. This axis is verified with the well known ground state splitting of the D_1 and D_2 lines. The cross section, σ, cell length, l, and the number density, n, make up the y-axis termed absorbance, σln. The lineshapes shown in this section for the probe are only for basic understanding while in Chapter 4 the probe lineshapes vary significantly and require necessary understanding.

4.1. Pump Beam near 894nm (D_1)

The D_1 pump beam is pressure broadened approximately 75 MHz and blue shifted approximately 40 MHz according to Pitz [13]. The pump beam's spectral location for all results is fixed on the peak of the left lineshape as indicated by the circle in Figure 10. The splitting of the each hyperfine structure is also shown for clarity which was generated at 35˚C and near zero pressure. The pump laser was scanned 20 GHz over 120 seconds to capture the D_1 transition lineshapes. The pump power incident to the heat pipe has been measured to be on the order of 50 mW. As visible in Figure 10 the cell is opaque when spectrally located on line center of the D_1 transition.

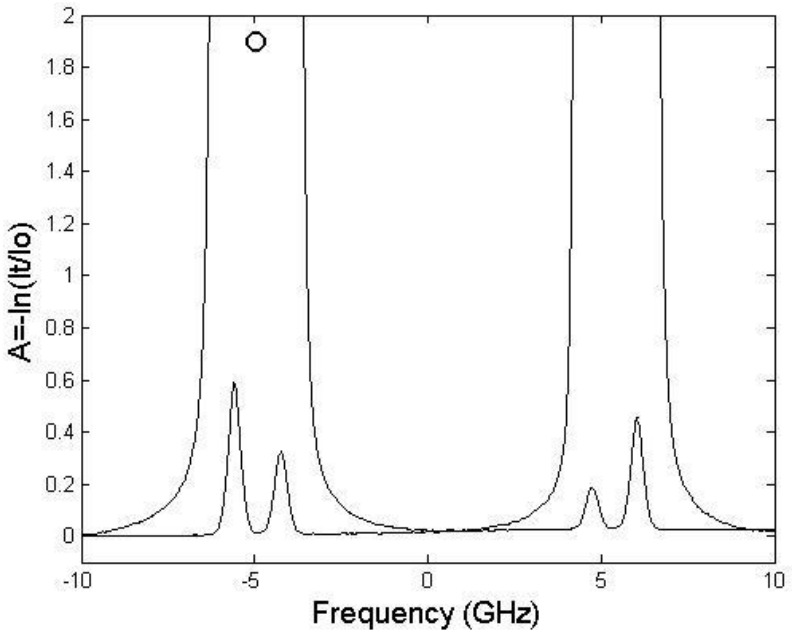

Figure 10: The cesium lineshapes pressure broadened with 5 Torr N_2 at 75˚C for the D_1 transition and a near zero, 35˚C hyperfine splitting set of all 4 distinct lineshapes.

The pump beam is fixed in location for the results given. The pump beam is approximately located at x = 10 mm while the probe scans from 0-15 mm across the heat pipe. The pump beam is modulated manually in some results through a beam block being placed in the pump beam path prior to heat pipe entry. The pump powers used are much larger than that of the probe to ensure the pump heating is beyond dominant, forcing the probe heating to be insignificant. The pump lineshape is considered to be a function of the temperature and pressure. The pressure and temperature are given for each result to ensure clarity of the variables and constants throughout each experiment.

4.2. Probe Beam near 852nm (D_2)

The D_2 hyperfine structure of the probe is pressure broadened approximately 100 MHz and blue shifted approximately 30 MHz provided by Pitz [8]. The probe frequency

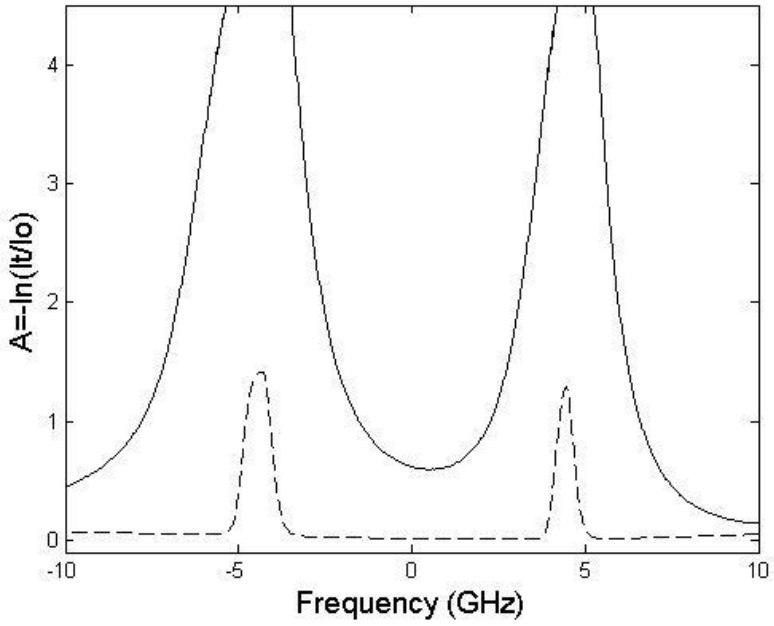

Figure 11: The cesium lineshapes pressure broadened with 5 Torr N_2 at 75˚C with a near zero pressure, 35˚C reference denoted by the dashed line for the D_2 transition.

can be known precisely while the absorption varies depending on temperature. The spectrum shown in Figure 11 is taken with the pump off and at a heat pipe spatial location of 13 mm. The probe has been spectrally scanned 20 GHz over 80 seconds to effectively capture the D_2 lineshapes. The probe power is on the order of 5 μW. The probe lineshapes in Figure 11 are also opaque shown by the solid line while the dashed line is a lower pressure and temperature and only differs from the pump due to the significant reduction in power.

IV. Results and Analysis

1. Spatial Scans with Pump Off and On Repeatedly

A spatial scan of the heat pipe has been produced with the aid of the motorized translation stages and a manual switch to turn the pump laser on/ off. The spectral locations of the pump and probe have been fixed for the results in Figure 12. The pump lies on the peak of the red lineshape at 335111.45 GHz (on line center) and probe lies on the left side of the peak of the red lineshape at 351720.0 GHz (-2 GHz from line center). The pressure and temperature of the heat pipe are 5 Torr N_2 and 70˚C respectively. The pump has been turned off and on during the spatial scan to instantaneously measure the probe absorbance values at locations throughout the heat

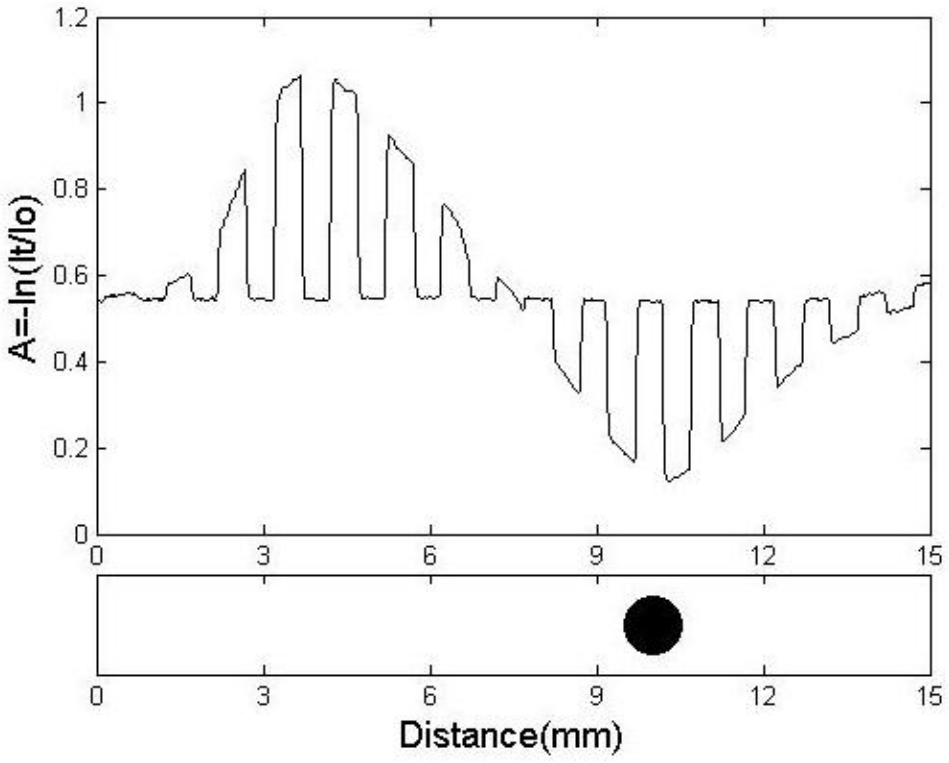

Figure 12: Spatial scan of heat pipe with pump on/ off repeatedly with probe located at 351720.0 GHz (-2 GHz from line center)

pipe when the pump laser is heating the gaseous medium. The pump location spatially is positioned at approximately 10.5 mm on the x-axis, as shown in Figure 12 by the large black dot on the lower plot. The sinusoidal resembling data is that of the pump on while the flat line data is the pump off. This data is not to be mistaken to be symmetric, like once thought, as later experimental data shows otherwise with valid reasoning. The pump has been switched on and off repeatedly every 0.6 mm of the spatial scan to instantaneously obtain the absorbance at each spatial location with the pump on/ off. The pump power in/out of the heat pipe is 53 mW/ 33 mW while the probe power in/ out are 22 μW/ 5 μW. The losses at the windows are approximately 12 μW for the 22 μW incident.

Figure 12 is of significant importance to this document due to the direct observation that, when the pump is on, the heat pipe volume experiences an instant change in the cesium number density. The diameter of the studied region of the heat pipe is given on the x-axis where x = 0 mm and x = 15 mm are near to the heat pipe walls. The absorbance with the pump off has an approximate value of 0.55 as indicated by the y-axis. The pump on values of absorbance ranges from about 0.1 to 1.1, which is a significant gradient that develops due to the laser load heating the gaseous medium. The volume that the pump interrogates has a decrease in absorbance by a factor of around 5 while an increase in absorbance by a factor of 2 is observed in the 0-7 mm region of the heat pipe. These effects make intuitive sense because the number density in the heat pipe volume is considered constant with the pump off and on. When the pump is on, the number density is decreased near the pump volume which must result in an increase in number density elsewhere in the heat pipe, which is observed in Figure 12.

Similar experiments to that shown in Figure 12 have been produced giving results shown in Figure 13 and Figure 14. The pump location has been fixed for both spatial

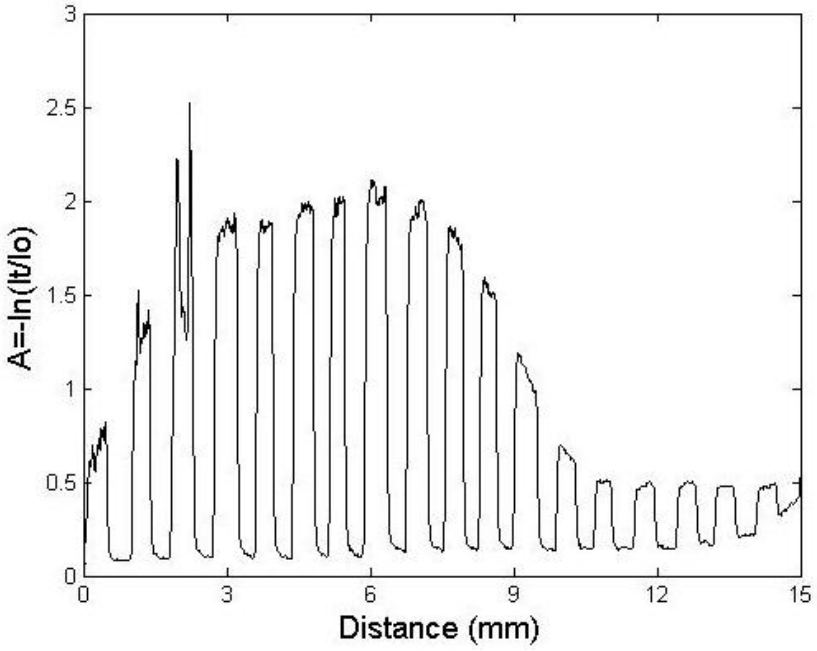

Figure 13: Spatial scan for probe at 351716.8 GHz (-5.2 GHz from line center)

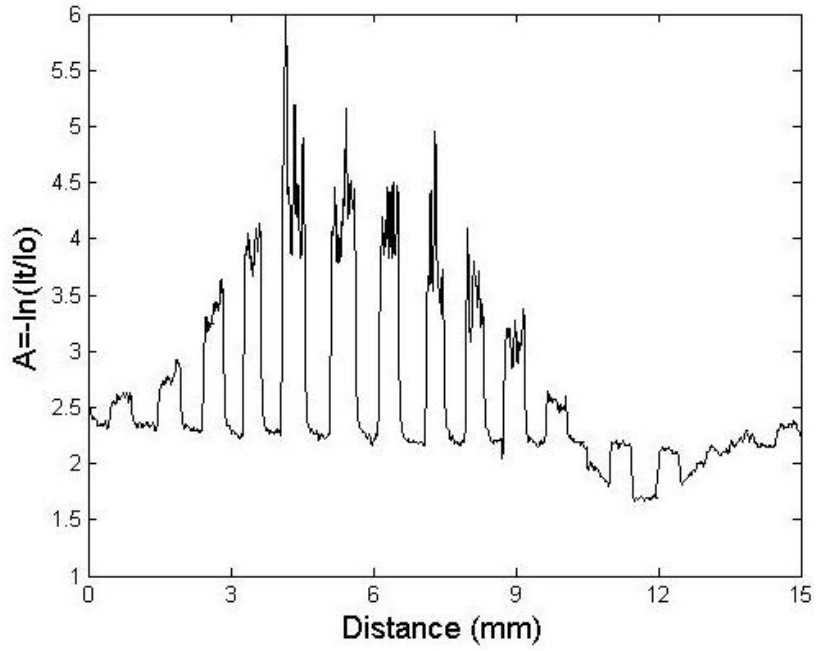

Figure 14: Spatial scan for probe at 351720.4 GHz (-1.6 GHz from line center)

scans in location and frequency while the probe frequency has been changed from 351716.8 GHz (-5.2 GHz from line center) in Figure 13 to 351720.4 GHz (-1.6 GHz from line center) in Figure 14. These two images have slightly different results. The difference can be explained further by the location of the probe on the D_2 lineshapes.

The probe frequency has been changed to 351720.5 GHz (-1.5 GHz from line center) to gain information on the probe frequency dependence on the number density gradients. Figure 14 shows the results of this experiment having an incident probe power of 1 μW and an incident pump power of 25 mW. The pump again has been turned off and on repeatedly to instantaneously gain information about pump influence. In both Figure 13 and Figure 14 the trends are similar in that inside the pump volume (x = 11.5 mm) has a much lower Cs number density than that of the volume where the pump is not present (x = 5.5 mm). The experiments shown in Figures 13 and 14 are only two of several data sets showing the same trends. Appendix A contains several additional spatial scans for several probe frequencies and an additional probe power as noted.

2. D_2 Lineshapes for several heat pipe locations

The number density gradients that have been shown to develop inside the heat pipe are directly related to temperature. The lineshapes are given in Figure 15 to help aid understand the number density gradients. The D_2 lineshapes of the probe are given for 6 different heat pipe locations. These lineshapes were created with the use of a signal generator to modulate the frequency back and forth across the D_2 hyperfine structures. The pump power in/out is 25 mW/ 12 mW while the probe incident power is approximately 1 μW. The external heat pipe temperature remains at 70˚C and the pressure inside is 5 Torr N_2. The 6 heat pipe locations have been overlaid to visualize the

differences inside and outside the pumped volume. Figure 15 is explained in more detail by dividing it into two parts: The left lineshape shown in Figure 16 and the right lineshape show in Figure 17.

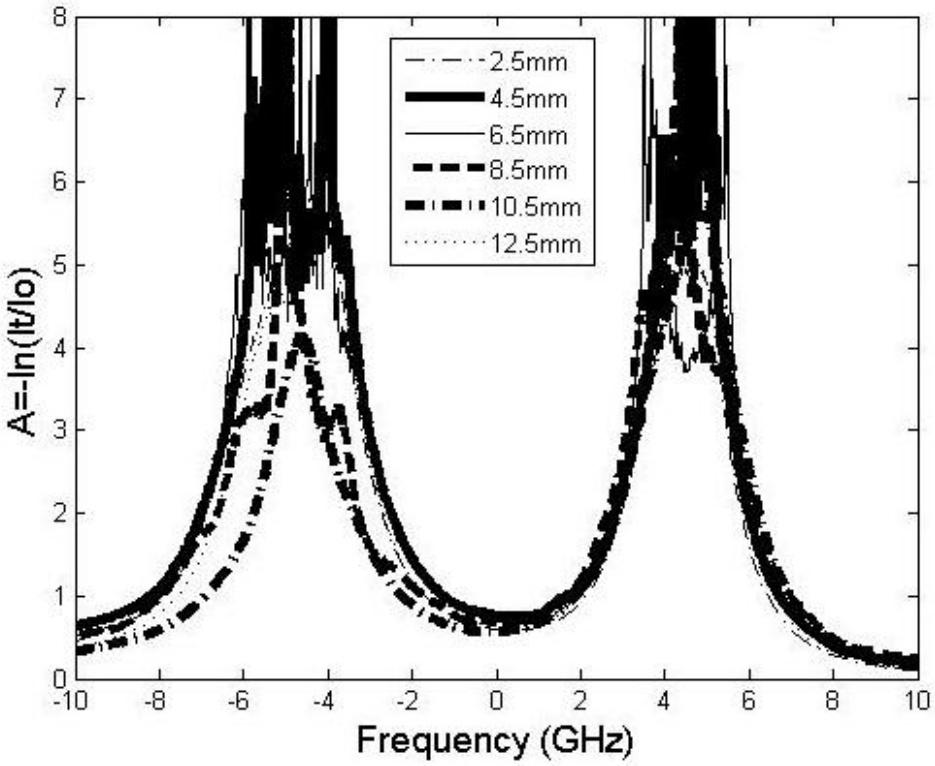

Figure 15: Lineshapes for 6 heat pipe locations

Many observations can be made from these two figures involving the shape, amplitude, width, and heat pipe location dependency on number density. In Figure 16 the absorption outside the pump beam (x = 4.5 mm) is much higher than the lineshape inside the pump beam (x = 10.5 mm). This is due to a depletion of the population of this excited state in the pump volume, leaving less Cs in the ground state. As the lineshapes are taken outside the pump, the ground state has not been depleted because there is no pump laser present. The low signal to noise shown for the lineshapes outside the pump beam is due

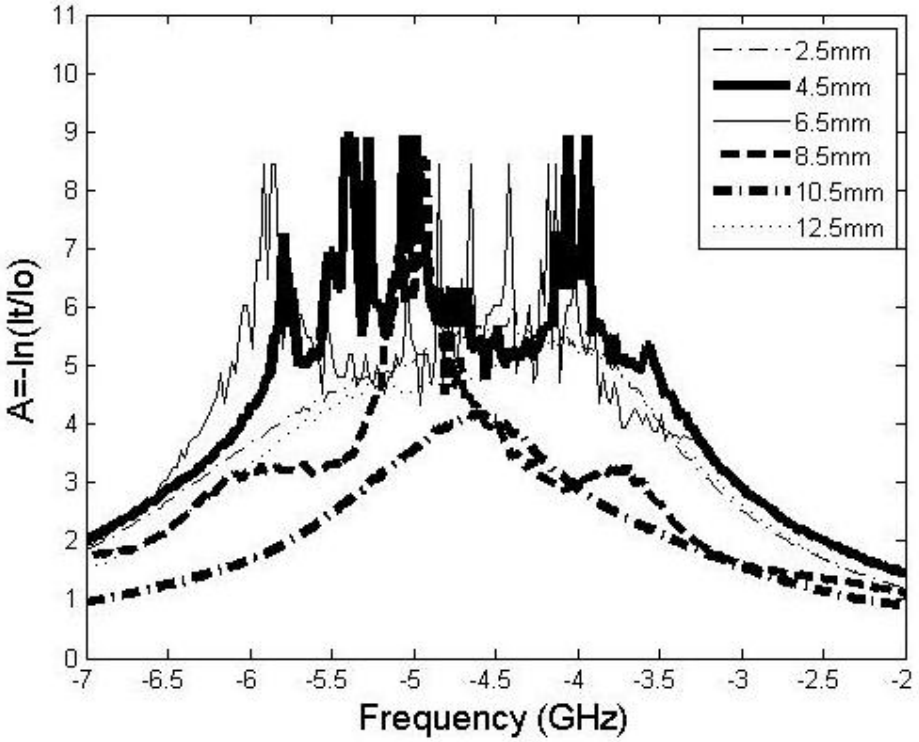

Figure 16: Left D_2 Cesium hyperfine structure

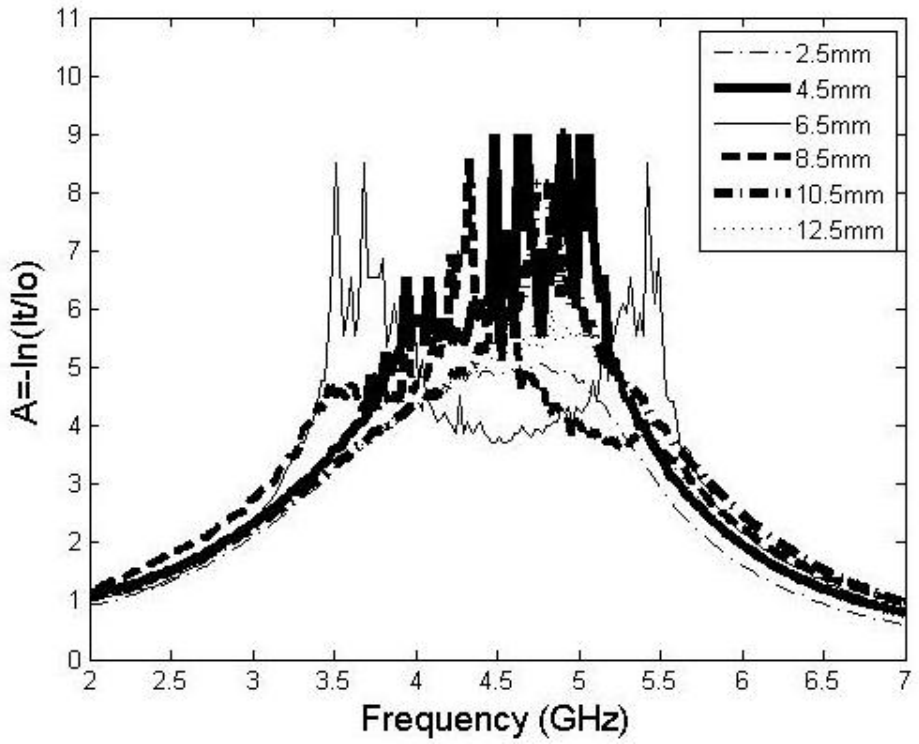

Figure 17: Right D_2 Cesium hyperfine structure

to high absorbance values. The high absorbance values make it known that there is a high number density at this location through Equation 3. The Cs excited state shown in the right D_2 cesium hyperfine structure has no depletion by the pump and the differences observed are due to an effect other than population changes. The Gaussian FWHM, given by Equation 9, is a function of the square root of temperature and several other constants. The Gaussian part of this Voigt lineshape in Figure 17 does have significant differences for the heat pipe locations. The dashed dark line, dash dot line, and the thin solid line all have a width greater than the solid black. The solid black is outside the pump has a smaller width than the others due to the low temperature at this location in the heat pipe. The dash dot and dotted line have the wider widths due to the heated gaseous volume via the pump laser. The effects here bring an additional method to verify that there is indeed a thermal gradient. In addition to the lineshape widths having a noticeable difference for various heat pipe locations, the amplitudes show that the high number density, in comparison to the pumped volume, is shown to be present outside the pumped volume.

The pump laser is indeed depleting the ground state only within the volume that is interrogated by the pump laser. The left half of the left hyperfine structure for several heat pipe locations is given in Figure 18. This plot clearly shows that the x = 10.5 mm heat pipe location has less population in the ground sate while the volume outside the pump beam has no depletion. A region has been zoomed in on to show the wing lineshape in more detail. Appendix A contains individual lineshape for the 6 heat pipe locations.

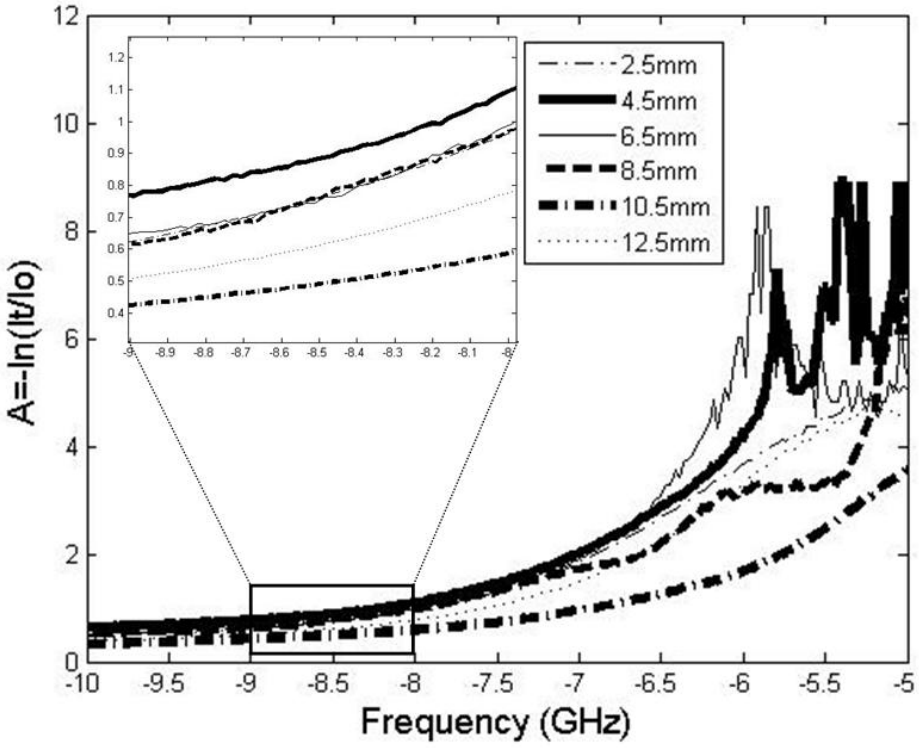

Figure 18: Left lineshape and zoomed section

3. Spatial Scans for Various Heat Pipe Wall Temperatures

The temperature has been varied in figure 19 from 50˚C, 75˚C, & 100˚C to vary the cesium concentration for the pump on and pump off spatial scans shown while the pressure is held at approximately 5 Torr N_2. The probe location has also been changed for each temperature to maintain a constant probe absorbance through the medium. The 50˚C, 75˚C, and 100˚C probe frequencies are 351722.1 GHz (+0.1 GHz from line center), 351720.0 GHz (-2.0 GHz from line center), and 351718.5 GHz (-3.5 GHz from line center) respectively. The pump on and pump off spatial scans across the heat pipe for these three temperatures are shown in Figure 19. This data shows how the number density gradient increases with a decrease in heat pipe wall temperature. The 50˚C

spatial scan has drastic differences in absorbance throughout the heat pipe while the 100˚C wall

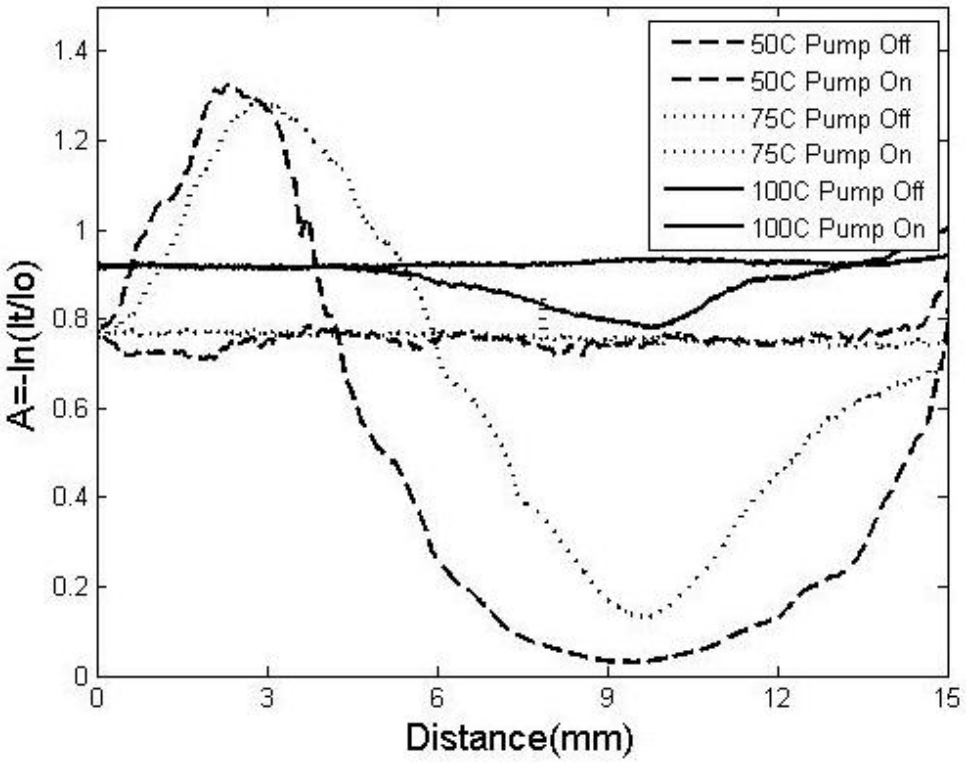

Figure 19: Pump on/off scans for 3 different alkali concentrations

temperature data has much less of an absorbance gradient /number density gradient. The pump is located at approximately 10.5 mm for each of the three spatial scans. This experiment did not modulate the pump on/ off as prior figures similar have; instead a spatial scan with the pump on was obtained followed by a pump off spatial scan. The heat pipe plays a significant role on the number density gradients present in the gaseous medium. As the heat pipe wall temperature approaches the pumped volume temperature, the thermal gradients are observed to diminish.

4. Absorbance Change inside Pump Volume for Varied Pump Power

The pump spectral location remains the same in Figure 20 as shown by the dot in Figure 10 and the probe spectral location is at 351720.2 GHz (-1.8 GHz from line center). The pump power is initially at 21 mW and is increased, with the aid of a neutral density wheel, to 38 mW represented by the x-axis in Figure 20. The pump power out of the heat pipe was measured to be 16 mW when the incident was 38 mW. The absorbance versus pump power inside the pump volume spatially is shown. This plot directly shows that the increase in pump power results in a decrease in absorbance. This trend has been observed in all data previously for 0 mW pump power as a reference to the pump being

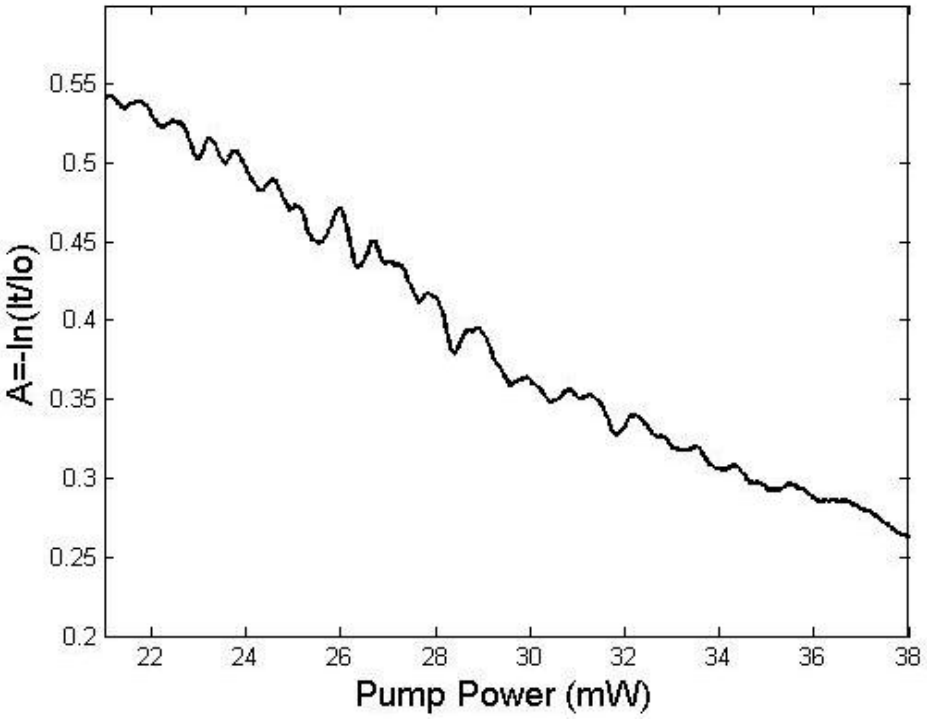

Figure 20: Probe fixed at 351720.2 GHz (-1.8 GHz from line center) spectrally and spatially inside pump spatially for varying pump power monitoring probe absorbance

on some location on this data set. The pump power in/out is 38 mW/ 16 mW while the probe power in/out is 188 µW/ 6 µW. This data is taken at 70˚C and agrees with the

absorbance values shown in Figure 12. This data should not be taken as linear due to the pump power being manually varied and the neutral density filter used does not linearly decrease pump power.

5. Absorbance Change inside Pump Volume for Varied Nitrogen Pressure

Positioning the probe to be inside the pump volume and varying only nitrogen pressure leads to the results shown in Figure 21. The pump spectral location is indicated by the dot in Figure 10 and is at 335111.45 GHz (on line center). The probe is located at 351721.3 GHz (-0.7 GHz from line center). The temperature of the heat pipe walls is 50˚C and the power in/out for the pump and probe are 37 mW/ 21 mW and 20 µW/ 5 µW respectively.

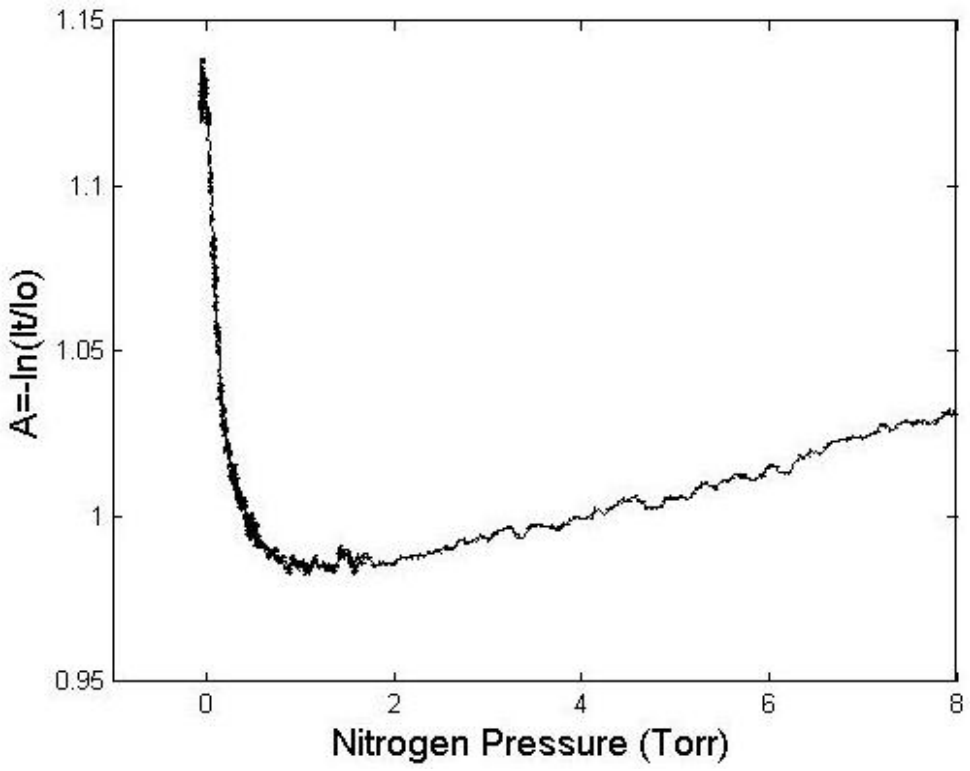

Figure 21: Probe fixed at 351721.3 GHz (-0.7 GHz from line center) spectrally and spatially inside pump while N2 pressure varied from 0-8 Torr

6. Pump off spatial scan across heat pipe

The heat pipe has been spatially scanned with the pump off to observe number density gradients that are in the background and wall diffusion effects. Figure 22 provides insight about the diffusion of cesium from the heat pipe walls in the evaporator section of the heat pipe. The spatial scans previously presented only look at the central 1.5 cm of the heat pipe that have a clear path and no wall effects or partial probe beams in the entry region. As visible in this plot, there is a symmetric effect near the heat pipe walls that could be a combined effect of two things. As the probe enters the heat pipe, only part of the beam is being absorbed until the entire Gaussian probe beam is passing through the heat pipe at x = 0 mm. Another effect could be that the Cs diffusion from the heat pipe walls is significant due to higher temperature at the walls when the pump is off. This spatial scan is at 50˚C and low pressure. The effects shown here have only been

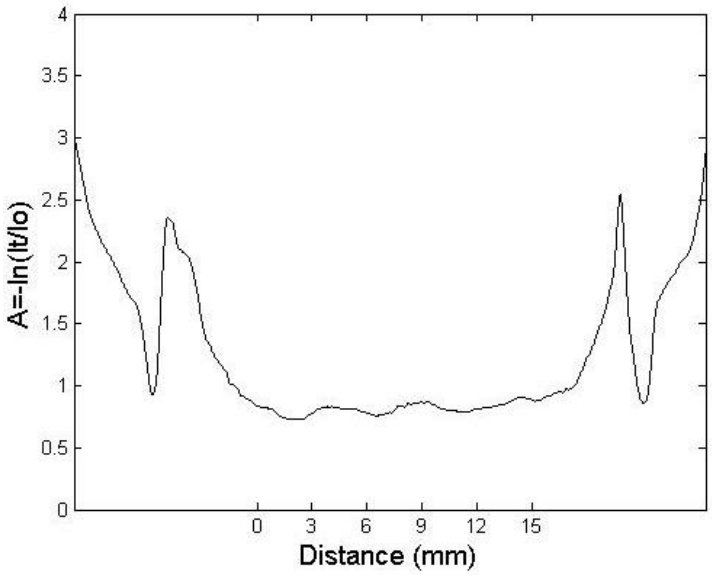

Figure 22: Spatial scan with pump off for Cs diffusion observations

present at low heat pipe temperatures and disappear at higher temperature. Most of the presented results are taken at temperatures where this is not significant or visible.

V. Discussion

1. Experimental Data Compared to Analytical Model Predictions

The experiments carried out in this research can be compared to the model predictions made by Zhu in 2010. The second order nonlinear differential equation, Equation 4, proposed has been solved with constants more suitable for this research. Zhu had several pump powers and used 500 Torr helium while this research is mainly 5 Torr N_2 and pump powers around 40 mW. The thermal conductivity and heat deposited into the system have been loosely calculated to simply obtain a rough thermal gradient. This estimation is done with the laser load heating at the center of the heat pipe with a radius of 7.5 mm. The temperature inside the heat pipe is estimated to about 550˚C while the

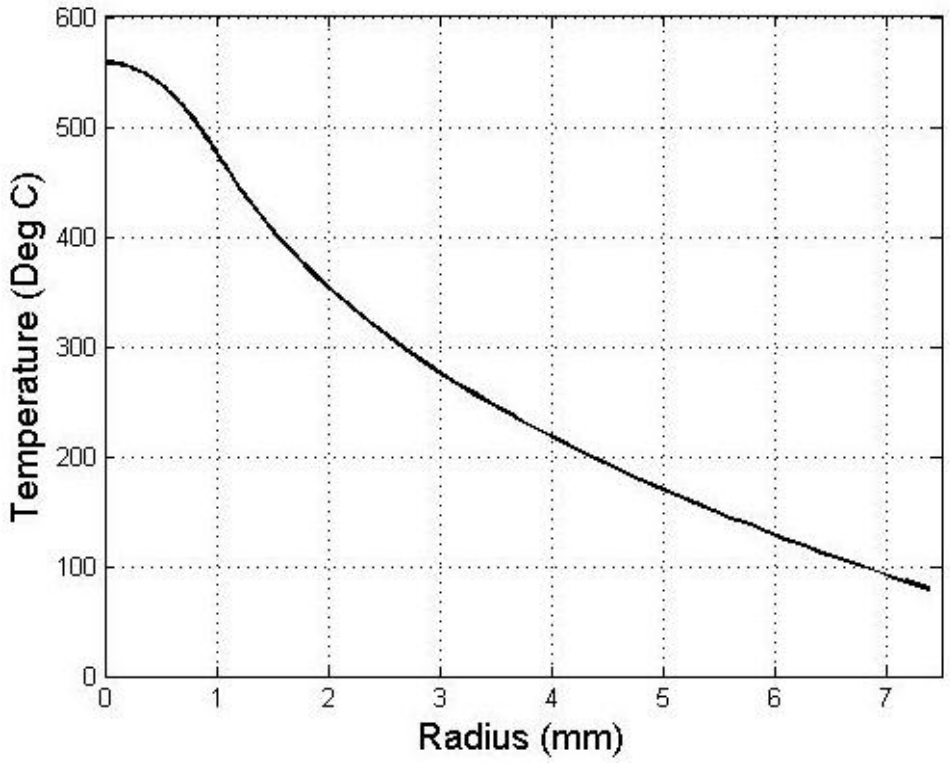

Figure 23: Proposed thermal gradient by Zhu's model for 75˚C heat pipe wall temp, 20 mW incident, η of 0.71, and radius of 7.5 mm.

wall temperatures were set to 75˚C as the x = 7.5 mm temperature indicates. The pump beam has been taken to have a beam waist with a radius of 1mm. The P_{in} value has been set to 20 mW while the estimated η is 0.71. The q_v term is simplified and given as:

$$qv = \frac{P_{in}\eta}{\pi * w_p{}^2} \tag{12}$$

where P_{in} is the power incident, w_p is the radius at the beam waist, and η is an efficiency factor. The longitudinal thermal gradients have been eliminated and the absorbsion efficiency disregarded. The thermal conductivity can be approximated via Sutherland's Formula given by:[5]

$$k = k_o \frac{T^n}{T_o} \frac{T_o + S}{T + S} \tag{13}$$

where k_o is the reference thermal conductivity, T_o is the reference temperature, n is a power constant, and S is a temperature constant. The estimated q_v is 4520 W/cm^2 while the thermal conductivity is estimated by Equation 13, known as Sutherlands Equation [5]. The k_o and T_o used in this equation are 24.2 mW/m-K and 273 K respectively while S and n are 150 K and 1.5 respectively. The thermal conductivity is calculated to be 0.488 W/m-K. The thermal gradients suggested by this model are not far from what actually may be presented in this data.

2. Temperature obtained from absorption values

The temperature inside the pump beam and outside the pump beam can be suggested from the absorption values at these locations inside the heat pipe with a few major assumptions. The spatial scan shown in Figure 14 is used to determine absorption values

inside and outside the pump and attempt to back out a temperature. The absorbance values inside the pump and outside the pump are estimated to be 1.75 and 4.5 respectively in Figure 14. The absorbance relationship to the path length, cross section, and number density is utilized to back out an approximate temperature for the two regions. Assuming the cross section and path length are both constant, which they are not, we can say that the absorbance is proportional to the number density given by:

$$A \sim (\sigma l) n \tag{14}$$

where l is the path length, n is the number density, and σ is the cross section. The number density can be assumed as related to temperature through the inverse relation given by:

$$n \sim \left(\frac{P}{k}\right)\frac{1}{T} \tag{15}$$

where T is temperature, P is pressure, and k is the Boltzman's constant. The partial pressure of cesium is assumed to be constant throughout the volume, which may or may not be true. Combining Equation 14 and 15, we obtain a relationship suggesting that the absorbance is inversely proportional to the temperature given as:

$$T \sim \left(\frac{\sigma l P}{k}\right)\frac{1}{A} \tag{16}$$

where A is the absorbance. With the assumptions mentioned we can simply group all the constants into one term and use the initial conditions to determine the constant. The initial conditions are that the wall temperature is known. At a known heat pipe wall

temperature of 70˚C (343K), and absorbance of approximately 2.25, the constant is roughly 772. With this constant and the two absorbance values known from the spatial scan, a temperature can be estimated for the two distinct locations in Figure 14. The high temperature inside the beam is approximated to be 170˚C (443 K) while the medium outside the beam is approximated to be -100˚C (173 K). This approximation method does not account for a major factor in the temperature profile that needs to be taken into account and is therefore not close to the true effects and should not be used in determining the thermal profile. Adding heat to the system, assuming a constant number density, will increase the average temperature of the entire gaseous medium. This is assumed to cause the pressure of the entire medium to increase some ΔP, and assumed to greatly influence the temperature profile. Another suggested approximation for the temperature profile as a function of radius is given as:

$$T(r) = \left(\frac{P'}{P_o}\right)\left(\frac{\bar{A}}{A(r)}\right)T_o \tag{17}$$

where P' is the pressure rise due to the pump laser on, P_o is a reference pressure, A is the absorbance, $\bar{A}$ is the average absorbance with the pump on and T is the temperature. The P prime is define as $P_o + \Delta P$ where P_o is the pressure of the heat pipe with no heating by the pump laser and the ΔP is the increase in pressure by the pump laser. To achieve temperatures as high as Zhu's model inside the pump, the pressure ratio term (P'/P_o) is approximated to be about 2.6 if it were the driving factor for the wrong assumptions previously mentioned. An experiment has been carried out following the pressure analysis yielding results indicating the pressure term has no visible change.

3. Future Work

This work has experimentally determined heat pipe gradients when heating a gaseous medium with a pump laser while model predictions have currently been relied upon. The once thought major dependant variables on the thermal gradients have shown influence while many assumed constant variables may be significant to the thermal gradients. Additional attention is needed on the dependence of the heat pipe wall temperature, cross section, pressure increase by pump laser, gain length changes, pump induced losses, and the collisional partner influence used in the DPAL system. Further optimization of heat pipe fabrication is necessary to improving the control of the experimental analysis while lasing remains feasible. Experimental data collected in this research is in need of comparison to well known lineshape equations to predict the thermal gradient necessary to create a detectable and accurate thermal gradient.

The convolved Voigt lineshapes can be predicted for several temperatures and then compared to the lineshapes shown in this work to determine the validity of a thermal gradient. The FWHM can be used to extract a quantitative temperature enabling values to be compared for the predictions of the model to actual experimental data. This research focused more on one wall temperature, one nitrogen pressure, and low pump laser powers. A set of lineshape at several heat pipe locations while varying the heat pipe wall temperature will allow for this variable to be further explained while an additional set of lineshapes for various nitrogen pressures will resolve the nitrogen pressure dependence on the gradients developed in the heat pipe. Expanding to several buffer gasses will allow for an optimized gas that minimized a number density gradient.

The current thermal gradient models for DPALs may help determine how significant the thermal gradient affects performance and what variable can be actively controlled to increase performance. The longitudinal axis thermal gradients have only been predicted to be significant in models while experimental data is currently not yet been demonstrated. Once thermal gradient dependence is known clearly, the power scaling predictions for DPALs can then be optimized and greatly benefit future thermal management problems that have been shown to occur in past laser systems.

The lineshapes are truly an accurate way to gain lots of information about population, temperature, number density, absorbance, and will allow for dependence on cross section to be determined. A series of experiments obtaining the lineshapes as a function of heat pipe radius for each dependant variable will close in on the true mechanics driving gradients throughout the heat pipe while heating with a pump laser.

VI. Conclusion

This research has began to characterize the radial thermal distributions that have only been predicted and suggested by models to be of significant effect when heating a gaseous medium with a laser. The demonstrations suggest that the thermal gradients have a significant influence on the absorbance distribution. The absorbance values are shown to increase by a factor of 2 outside the gaseous medium axially heated by the pump laser while a decrease is observed inside the pump beam. Several absorbance distributions are presented suggesting development of high number density gradients across the heat pipe. The current DPAL demonstrations have not experimentally measured the thermal gradient behaviors until this research.

Spatial scans with a probe laser have provided evidence of significant absorbance differences throughout a cesium gaseous medium interrogated by a pump laser. The pump laser has been shown to increase the absorbance outside the pumped volume by at least a factor of 2 while the absorbance inside the pumped volume has been shown to decrease by a factor of 5. Several spatial scans have been generated leading to conclusions that a dependence on probe frequency and heat pipe temperature could be in existence. An increase in pump power has been shown to decrease the absorbance inside the pump while nitrogen pressure plays an important role.

The D_2 lineshapes have been shown to have a radial dependence throughout the heat pipe directly related to the temperature rise inside the pumped volume. The lineshape widths validate the absorption fluctuations across the heat pipe are indeed true. Diffusion of cesium from the heat pipe walls has been visible at low wall temperatures and shown to have no significance after well above the melting point of cesium. The current model

predictions have similar trends to that of this research qualitatively but not yet quantitatively. New model predictions have been proposed and require more research to accurately quantify the thermal gradients. Studying the thermal gradients experimentally becomes challenging when operating inside a heat pipe and requires cautious fabrication techniques.

Further studies on the heat pipe gradients are in need of attention to extract a true temperature, number density, and absorbance value for the pumped region accurately. Experimentally determining the lineshapes for several heat pipe locations while interrogating the gaseous medium via a pump laser has been determined the best was to investigate the heat pipe gradients. Absorbance gradients have been observed, however the temperature trends extracted have not yet made physical sense while number density gradients and cross section gradients have been shown to develop while the pump laser is on.

Appendix A. Supplementary Figures

Figures 24-27 are supplemental spatial scans at different powers and different probe frequencies. Figures 24 and 25 are at 1 µW while Figures 26 and 27 are at 2.8 µW.

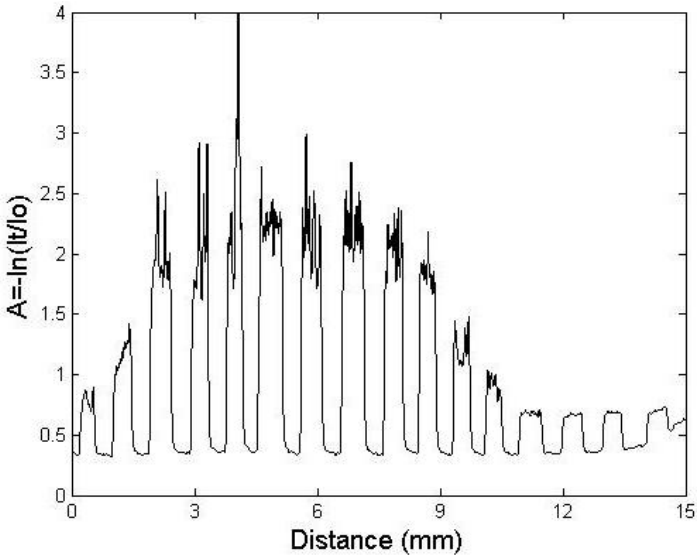

Figure 24: Spatial scan with probe fixed at 351718.2 GHz (-3.8 from line center) with 1 µW probe power incident

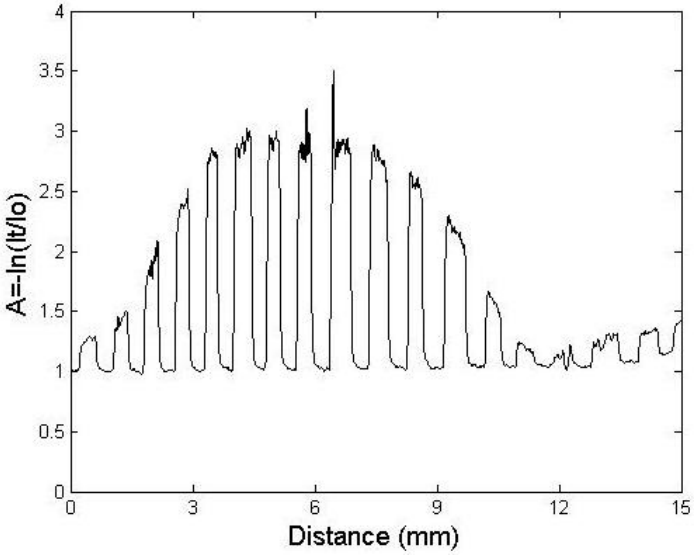

Figure 25: Spatial scan with probe fixed at 351719.5 GHz (-2.5 from line center) with 1 µW probe power incident

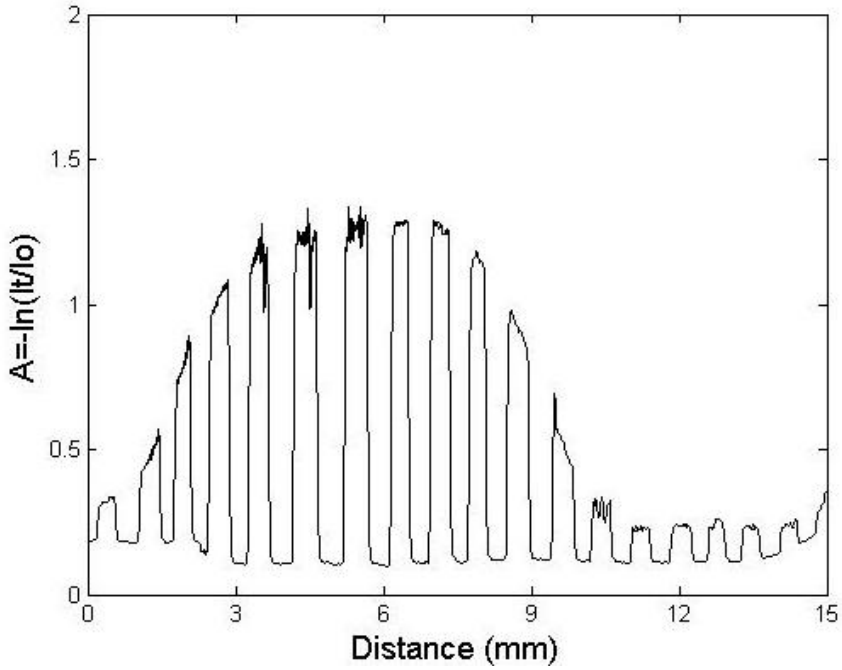

Figure 26: Spatial Scan with probe fixed at 351718.0 GHz (-4.0 from line center) with 2.8 μW probe power incident

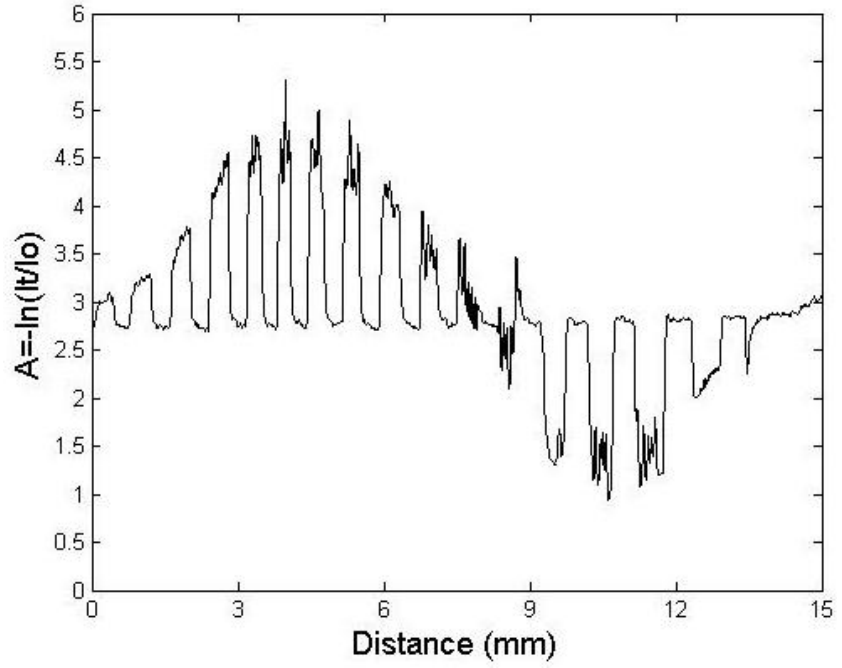

Figure 27: Spatial scan with probe fixed at 351720.4 GHz (-1.6 from line center) with 2.8 μW probe power incident

The D_2 linshapes are provided individually for several heat pipe locations in Figures 28-33. The width and amplitude of each is more clearly presented.

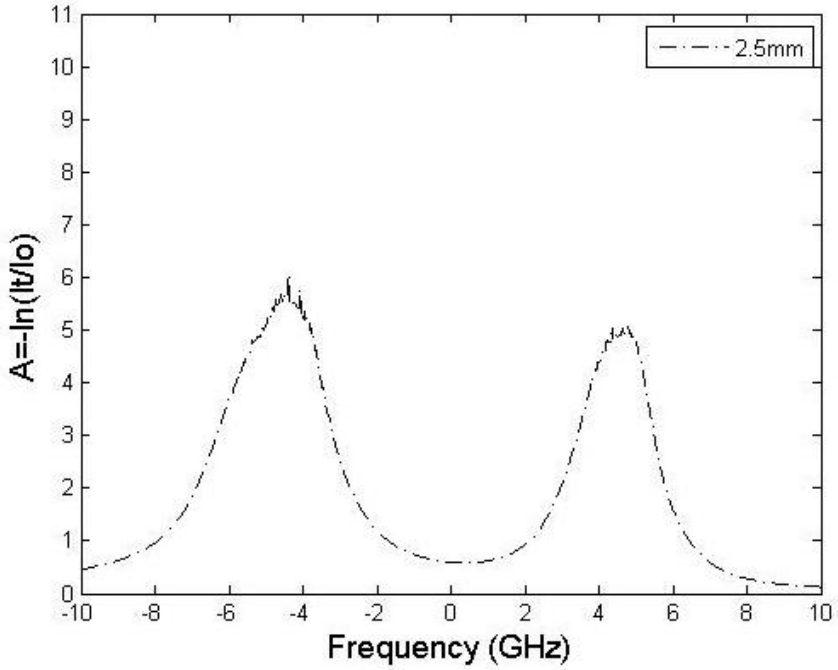

Figure 28: D_2 lineshape at location in heat pipe of x = 2.5 mm

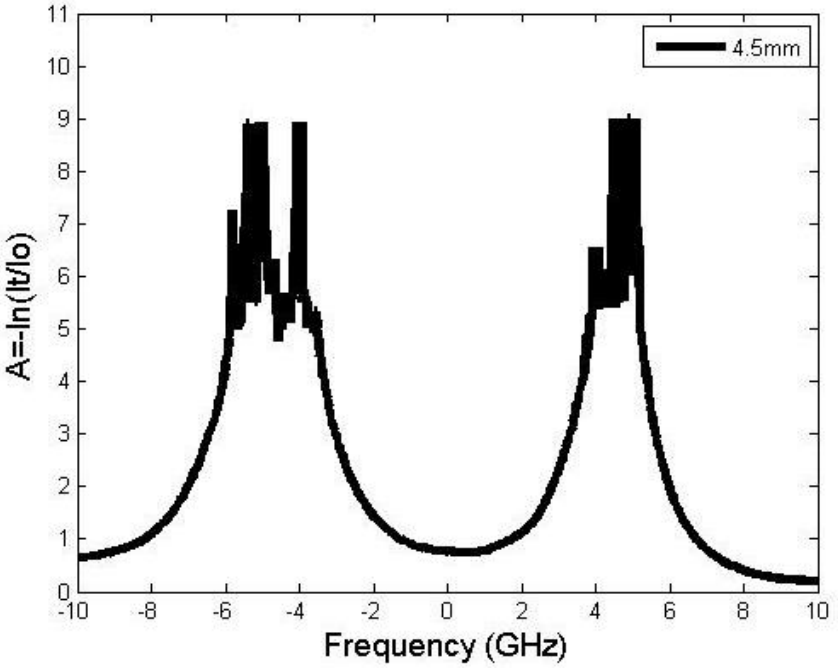

Figure 29: D_2 lineshape at location in heat pipe of x = 4.5 mm

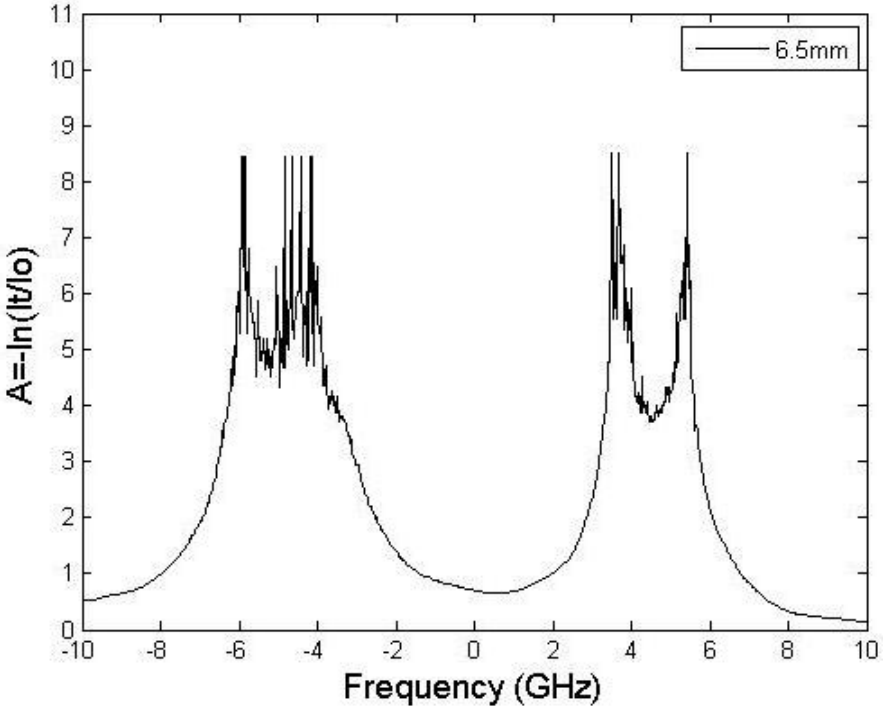

Figure 30: D_2 lineshape at location in heat pipe of x = 6.5 mm

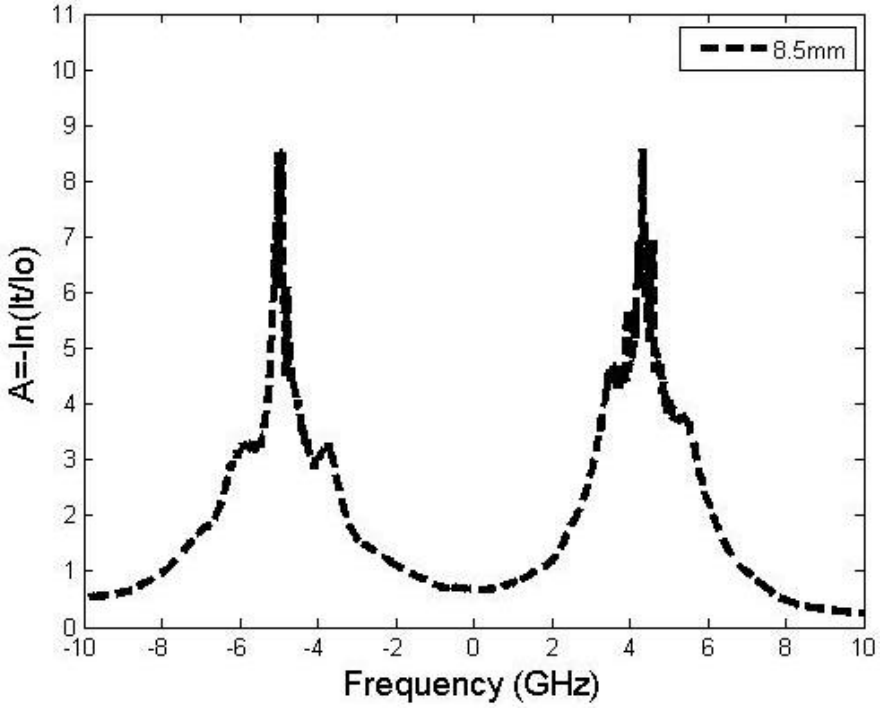

Figure 31: D_2 lineshape at location in heat pipe of x = 8.5 mm

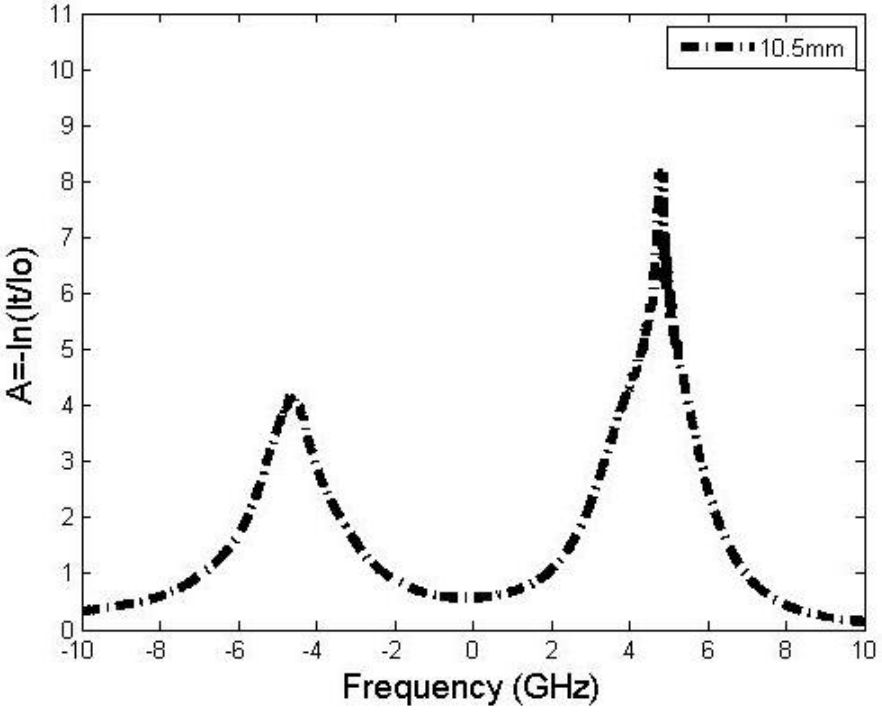

Figure 32: D_2 lineshape at location in heat pipe of x = 10.5 mm

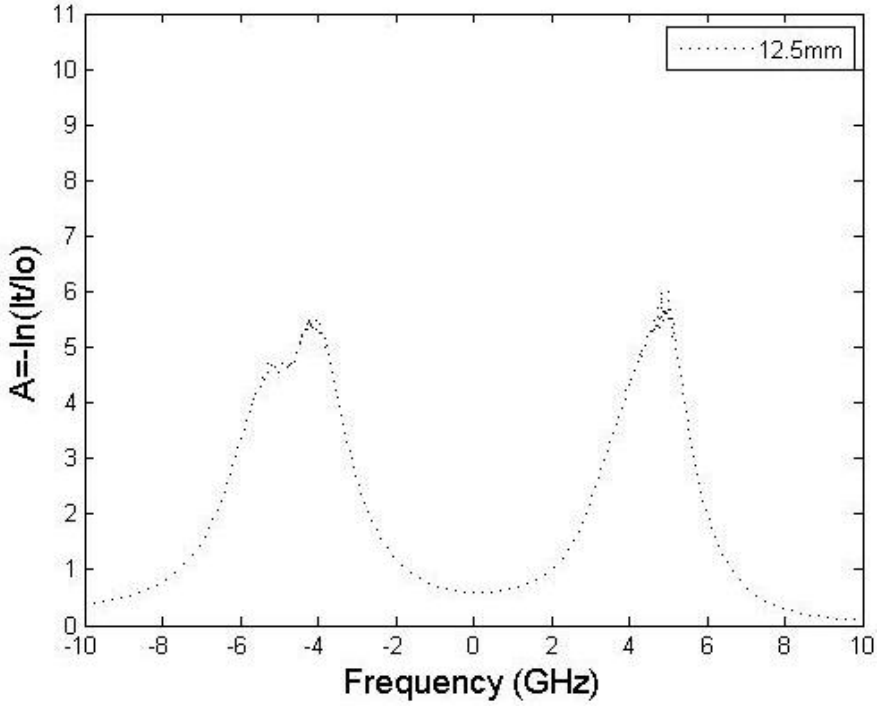

Figure 33: D_2 lineshape at location in heat pipe of x = 12.5 mm

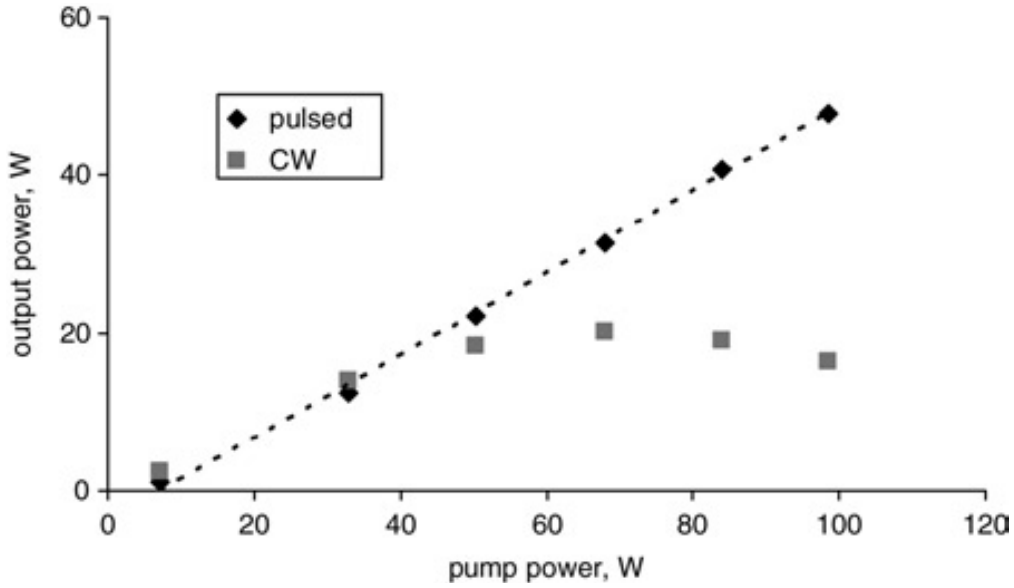

Figure 34: Pulsed DPAL versus CW providing evidence of thermal effects limiting the DPAL performance[17]

Bibliography

[1] Krupke, W., R. Beach, V. Kanz, and S. Payne, *Resonance transition 795-nm rubidium laser*, Optics Letters **28**:2336, 2003.

[2] Beach, R., W. Krupke, V. Kanz, and S. Payne, *Diode-Pumped Alkali Atom Lasers*, Lawrence Livermore Technical Report, UCRL-TR-210223, 2005.

[3] Zhu, Q., Pan, B., Chen, L. Wang, Y. and Shang, X., *Analysis of temperature distributions in diode pumped alkali vapor lasers*, Optics Communications **283**:2406-2410, 2010.

[4] Mills, A.F., *Basic Heat and Mass Transfer*, Production Co, Concord, MA, 1995.

[5] F.M.White, *Viscous Flow Theory*, pages 28-31 (2006).

[6] Bird, G.A., *Molecular Gas Dynamics and the Direct Simulation of Gas*, Oxford University Press, New York, New York, 1994.

[7] Bernath, P.F., *Spectra of Atoms and Molecules*, Oxford University Press, New York, New York, 1995.

[8] Pitz, G.A., Fox, C.D., and Perram, G.P., *Pressure Broadening and Shift of the Cesium D_2 transition*, Physical Review A **82**:042502, 2010.

[9] Peterson, G.P., *Introduction to heat pipes: Modeling, Testing and Applications*, John Wiley and Sons, New York, 1994.

[10] Faghri, A., *Heat Pipe Science and Technology*, Taylor and Francis Publishers, Washington D.C., 1995.

[11] Sulham, C.V. *Laser Demonstration and Characterization of Optically Pumped Alkali Laser Systems*, PhD Dissertation, Dept. of Physics, Air Force Institute of Technology, Wright Patterson AFB, OH, 2010.

[12] Andalkar, A., *Measurement of the coalitional self-broadening of the cesium $6S_{1/2} \rightarrow 5D_{3/2}$ (689-nm) electric quadrupole transition*, Physical Review A **70**:052703, 2004.

[13] Pitz, G.A., Wertepny, D.E., and Perram, G.P, *Pressure Broadening and Shift of the Cesium D_1 transition*, Physical Review A **80**:062718, 2009.

[14] Perram, G.P., *An Introduction to Laser Weapon Systems*, The Directed Energy Professional Society, Albuquerque, NM, 2010.

[15] Hostutler, D.H., Klennert, Wade L., *Power enhancement of a Rubidium vapor laser with a master oscillator power amplifier*, Optical Society of America **16**:11, 2008.

[16]Zweiback, J., Komashko, A., Krupke, W.F., *Alkali vapor lasers*, Proc. of SPIE **7581**:75810G-1, 2010.

[17]Zhdanov, B.V., Sell, J., and Knize, R.J., *Multiple laser diode array pumped Cs laser with 48 W Output power*, Electronics Letters **44**:9, 2008.

REPORT DOCUMENTATION PAGE

Form Approved
OMB No. 074-0188

1. REPORT DATE *(DD-MM-YYYY)*	2. REPORT TYPE	3. DATES COVERED *(From – To)*
24-3-2011	Master's Thesis	March 2010 – March 2011

4. TITLE AND SUBTITLE
Radial Distribution of Absorption in a Cesium Heat Pipe with Axial Laser Heating

5a. CONTRACT NUMBER

5b. GRANT NUMBER

5c. PROGRAM ELEMENT NUMBER

6. AUTHOR(S)
Fox, Charles Daniel

5d. PROJECT NUMBER

5e. TASK NUMBER

5f. WORK UNIT NUMBER

7. PERFORMING ORGANIZATION NAMES(S) AND ADDRESS(S)
Air Force Institute of Technology
Graduate School of Engineering and Management (AFIT/ENY)
2950 Hobson Way, Building 640
WPAFB, OH 45433-8865

8. PERFORMING ORGANIZATION REPORT NUMBER
AFIT/GAE/ENY/11-M09

9. SPONSORING/MONITORING AGENCY NAME(S) AND ADDRESS(ES)
High Energy Laser – Joint Technology Office / Ackermann, H.
901 University Blvd S.E. Suite 100
Albuquerque, NM 87106 harro.ackermann@jto.hpc.mil

10. SPONSOR/MONITOR'S ACRONYM(S)
HEL-JTO

11. SPONSOR/MONITOR'S REPORT NUMBER(S)

12. DISTRIBUTION/AVAILABILITY STATEMENT
APPROVED FOR PUBLIC RELEASE; DISTRIBUTION UNLIMITED

13. SUPPLEMENTARY NOTES

14. ABSTRACT
Diode Pumped Alkali Lasers (DPAL) have been scaled to greater than 100 W and exhibit slope efficiencies exceeding 80%, offering application for tactical laser weapons. The hybrid DPAL system combines efficient diode pumping with the good beam quality and thermal characteristics of gas lasers. Thermal effects on alkali concentration have been observed to degrade performance, while low speed flowing systems are in development. However, spatial gradients in temperature and concentrations have not previously been observed. In the present work, a 0.8 W/ cm^2 pump laser at the D_1 frequency heats the medium in a T=50-100C Cs heat pipe with 5 Torr nitrogen used for quenching. A 31 $\mu W/cm^2$ diode laser probes the spectral absorbance of the Cs cell on the D_2 transition with radial spatial resolution. The 300 kHz linewidth probe laser is scanned 20 GHz across the optically thick hyperfine structure, revealing absorbances of 1-5. The absorbance outside of the pumped volume is modulated by up to a factor of 2 when the pump beam is blocked, suggesting significant temperature gradients. The radial temperature profile is observed across the 1.5 cm pipe with resolution of 2 mm. The variation of pump power, nitrogen pressure, and heat pipe temperature has been provided showing distinct trends. Cesium D_2 lineshapes have been obtained for several heat pipe spatial locations with the pump laser actively heating the gaseous medium.

15. SUBJECT TERMS
Diode Pumped Alkali Laser, Thermal Gradients, Axial Laser Load,

16. SECURITY CLASSIFICATION OF:			17. LIMITATION OF ABSTRACT	18. NUMBER OF PAGES	19a. NAME OF RESPONSIBLE PERSON
a. REPORT	b. ABSTRACT	c. THIS PAGE			Perram, Glen P., Professor, ADVISOR
U	U	U	UU	68	19b. TELEPHONE NUMBER *(Include area code)* (937) 255-6565, ext 4504 (glen.perram@afit.edu)

Standard Form 298 (Rev. 8-98)
Prescribed by ANSI Std. Z39-18